AGU PUBLICATIONS

JGR

Journal of Geophysical Research: Atmospheres

RESEARCH ARTICLE

10.1002/2015JD023213

Key Points:
- The average of hygroscopic growth factor distributions was bimodal
- The hygroscopicity parameter κ of organics was estimated to be 0.14–0.19
- The details of hygroscopicity are important to CCN number concentrations

Supporting Information:
- Supporting Information S1
- Text S1

Correspondence to:
M. Mochida,
mochida.michihiro@g.mbox.nagoya-u.ac.jp

Citation:
Kawana, K., T. Nakayama, and M. Mochida (2016), Hygroscopicity and CCN activity of atmospheric aerosol particles and their relation to organics: Characteristics of urban aerosols in Nagoya, Japan, *J. Geophys. Res. Atmos.*, *121*, 4100–4121, doi:10.1002/2015JD023213.

Received 21 JAN 2015
Accepted 7 APR 2016
Accepted article online 9 APR 2016
Published online 23 APR 2016
Corrected 30 MAY 2016

This article was corrected on 30 MAY 2016. See the end of the full text for details.

Hygroscopicity and CCN activity of atmospheric aerosol particles and their relation to organics: Characteristics of urban aerosols in Nagoya, Japan

Kaori Kawana[1,2], Tomoki Nakayama[3], and Michihiro Mochida[1]

[1]Graduate School of Environmental Studies, Nagoya University, Nagoya, Japan, [2]Now at Institute of Low Temperature Science, Hokkaido University, Sapporo, Japan, [3]Institute for Space-Earth Environmental Research, Nagoya University, Nagoya, Japan

Abstract The size-resolved distributions of hygroscopic growth factor *g* and the ratios of cloud condensation nuclei (CCN) to condensation nuclei of atmospheric aerosols were investigated in Nagoya, Japan. The average of the distributions of *g* at 85% relative humidity was bimodal. The size-resolved mean κ derived from *g* showed an increasing trend with diameter: 0.17–0.33 at 24–359 nm. The κ values calculated from CCN activation curves were 37% higher than those derived from *g*. Only 9% of the 37% difference is explained by the difference in the κ of inorganics under subsaturated and supersaturated conditions, suggesting a contribution of organics to the remaining 28% difference. The size-averaged κ of organics (κ_{org}) was calculated as 0.14 and 0.19 by two different methods. The number fractions of CCN predicted from the hygroscopicity data over the range of 24–359 nm are loosely consistent with those observed if the size- and time-averaged *g* is applied to all particles (differences: −30% to +10%). This consistency improves if size- and time-resolved *g* and *g* distribution are used (differences: −19% to −3%). Whereas the number fractions of CCN predicted from the composition data are greatly underestimated if organics are assumed to be insoluble (differences: −64% to −45%), they are more consistent if κ_{org} of 0.14 or 0.19 is applied (differences: −10% to +14%). The results demonstrate the importance of the dependence of the *g* of particles on time and particle size and the hygroscopicity of organics for CCN number concentrations in the urban atmosphere.

1. Introduction

Aerosol particles in the atmosphere affect global climate by acting as cloud condensation nuclei (CCN) and by absorbing and scattering solar radiation. The presence of anthropogenic aerosol particles that act as CCN leads to an increase in cloud albedo and the prolongation of cloud lifetime [*Twomey*, 1977; *Albrecht*, 1989]. To date, among factors that affect climate change, there is a large uncertainty regarding radiative forcing by anthropogenic aerosols associated with cloud processes. Additionally, anthropogenic aerosols may also alter precipitation patterns and surface temperature structures [*Ramanathan et al.*, 2001]. Understanding the roles of aerosols as CCN is thereby crucial to predicting future climate.

The hygroscopic growth and subsequent CCN activation of aerosol particles are governed by their chemical composition and their size. Hygroscopicity is a factor other than surface tension that is controlled by composition, and it governs the particle's hygroscopic growth. The hygroscopicity parameter κ [*Petters and Kreidenweis*, 2007] is widely used to represent the hygroscopicity of aerosol particles and the chemical components therein. In atmospheric observations, the κ values of particles has in many cases been obtained from the hygroscopic growth factor (*g*) measured using a hygroscopicity tandem differential mobility analyzer (HTDMA) [*Rader and McMurry*, 1986] under subsaturated water vapor conditions. Alternatively, the κ value of particles has also been obtained from CCN activation diameters (d_{act}) measured using a CCN counter under supersaturated conditions. The κ values of chemical components can also be determined when the particle chemical composition is also available. In global aerosol models, the parameterization of particle hygroscopicity using κ was adopted to estimate changes in the number concentrations of CCN (N_{CCN}) and cloud droplets, and radiative forcing by aerosols [*Liu and Wang*, 2010].

To assess the relationship between the CCN activation of aerosols and their size distributions and composition, CCN closure studies have been performed for different environments: urban [*Gunthe et al.*, 2011], remote [*Chang et al.*, 2007], forest [*Rissler et al.*, 2004], ocean [*Mochida et al.*, 2011], polar region [*Lathem et al.*, 2013], and high-elevation [*Jurányi et al.*, 2010] sites. In these closure studies, the characteristics of

CCN activation represented by N_{CCN}, d_{act}, and critical supersaturation (s_c) have been predicted based on hygroscopicity, chemical composition, or a combination of these two, as well as the number-size distributions. Although consistency (within ~10% difference) with substantial simplifications, i.e., the use of bulk composition/hygroscopicity, has been claimed [*Bougiatioti et al*., 2009, 2011], predicted values have been inconsistent with the measured in some studies, showing that the CCN activity cannot be predicted with simplified assumptions. In the latter case, more detailed properties and/or mechanisms than those considered in the predictions may be important [*Quinn et al*., 2008; *Moore et al*., 2012].

These closure studies indicate the importance of understanding the factors that control CCN activation and shed light on three important subjects to investigate. One is the estimation of the hygroscopicity of organics. This subject is important because the prediction of N_{CCN} and that of aerosol indirect radiative forcing is sensitive to the hygroscopicity of organics if the fraction of organics in aerosols is large [*Wang et al*., 2008; *Mei et al*., 2013a]. The estimated κ_{org} for atmospheric aerosol particles is variable: <0.1 for fresh hydrocarbon-line organic aerosol (HOA) and biomass burning organic aerosol [*Petters and Kreidenweis*, 2007; *Martin et al*., 2011], about 0.1–0.2 for secondary organic aerosol (SOA) [*Mei et al*., 2013b], and about 0.2–0.3 for water-soluble organic matter [*Asa-Awuku et al*., 2010]. To date, the relation between κ_{org} values and the chemical type of organics is not well understood. Although correlations of κ_{org} to the O/C ratio or f_{44}, i.e., variables related to the degree of oxygenation, are reported based on laboratory and field studies [*Aiken et al*., 2008; *Jimenez et al*., 2009; *Chang et al*., 2010], the degree of correlation and the slopes of the regression lines largely differ among studies [*Duplissy et al*., 2011; *Moore et al*., 2011; *Alfarra et al*., 2013; *Lathem et al*., 2013; *Mei et al*., 2013a, 2013b].

The second and third subjects are, respectively, the difference in particle hygroscopicity under subsaturated and supersaturated conditions, and the contributions of size, composition, and mixing state to CCN number concentrations. Whereas some studies report that particle hygroscopicity under subsaturated and supersaturated conditions is similar (difference: within 30%) [*Duplissy et al*., 2008; *Carrico et al*., 2008], other studies report that they are dissimilar ($>30\%$). Possible reasons for the inconsistencies include a reduction in surface tension, the presence of sparingly soluble materials, the dependence of the activity coefficient of water on the solution concentration, and particle asphericity [*Wex et al*., 2009; *Good et al*., 2010a, 2010b; *Dusek et al*., 2011]. These factors may largely be attributed to organics, and their contributions may depend on the composition of organics and thus atmospheric environments. Regarding the factors controlling CCN number concentrations, some studies suggest that number-size distributions are more important than the composition and the solubility of organics for the prediction of N_{CCN} [*Ervens et al*., 2007] and that CCN activation is well represented by an average κ [*Rose et al*., 2010, 2011]. By contrast, some other studies suggest that considering size- and time-dependent κ values is necessary to ensure the consistency of CCN closure [*Kammermann et al*., 2010; *Kim et al*., 2011]. In the case of urban aerosols, the variations of chemical components, hygroscopicity, and mixing state may greatly influence CCN closure. *Wex et al*. [2010] reported that considering externally mixed conditions in addition to size-segregated chemical composition is necessary to ensure agreement between prediction and measurement under urban conditions in the presence of particles both in less hygroscopic and more hygroscopic modes. However, it has also been reported that the degree of consistency between prediction and measurement is independent of the mixing state assumption [*Fors et al*., 2011]. The cause of the difference is unclear, and further investigation of this point is required.

As explained above, clarifying the hygroscopicity of organics and assessing factors that govern CCN activation and CCN number concentrations remain important. In this study, a field observation of atmospheric aerosols was performed in Nagoya, an urban site in Japan, in early Autumn 2009. The following factors related to CCN activity and CCN number concentrations were measured: the number-size distributions, bulk and size-resolved chemical composition, size-resolved growth factor distributions, and size-resolved ratios of CCN to condensation nuclei (CN). Based on the observed data, the size- and time-resolved hygroscopicity and CCN activity of aerosol particles in Nagoya are characterized. Additionally, the κ values of both particles and the organic components are derived, and the differences in particle hygroscopicity under subsaturated and supersaturated conditions are investigated. Moreover, variations in g with size and time, g distributions, and the hygroscopicity of organics to the CCN number concentrations are assessed. Finally, the influence of organics on CCN number fractions via solute and surface tension effects is briefly discussed. Note that the hygroscopicity and CCN activity of Nagoya aerosols in summer were reported elsewhere [*Kawana et al*., 2014]. The highlights of the present work include the derivation of the size-resolved hygroscopicity of organics and the closure of the number fractions of CCN in the atmosphere.

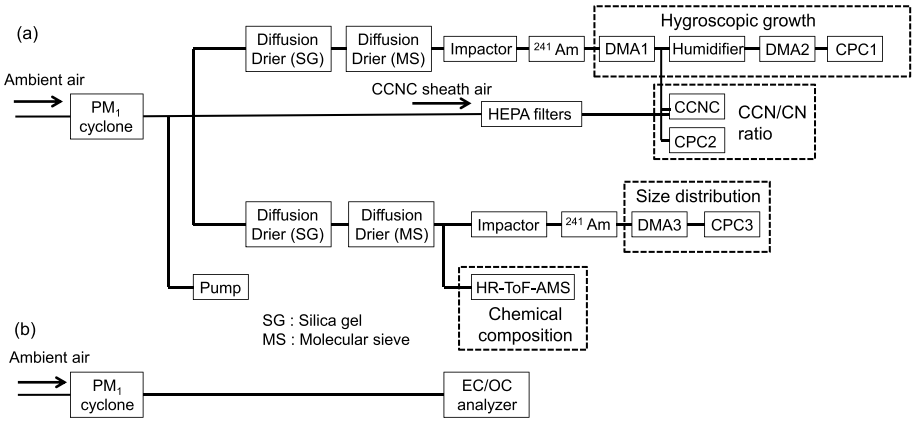

Figure 1. Schematic of the instruments.

2. Experimental Methods

2.1. Measurement

The observation of atmospheric aerosol particles was performed at the Higashiyama Campus, Nagoya University (35°09′N, 136°58′E) in the city of Nagoya, Japan, from 14 to 24 September 2009. Nagoya is the third largest city in Japan (population: 2.3 million) and is at the center of the Chukyo major metropolitan area (population: 9.1 million). The meteorological conditions and the concentrations of gaseous pollutants are explained in Text S1 and Figure S1 of the supporting information (SI). Five-day backward trajectories suggest that the air masses during the first 6 days were from the Sea of Japan and the Asian continent (Figure S2). They also suggest that air masses during the last 4 days passed over the coastal region of Japan that faces the Pacific Ocean.

A schematic of the observation instruments is presented in Figure 1. Aerosols were aspirated at two inlets placed 9.5 m above ground level and were passed through a PM_1 cyclone (URG2000-30EHB, URG) at a flow rate of 16.7 L min^{-1}. The aerosol in one of the sampling lines was introduced into a system consisting of an HTDMA and a CCN counter (CCNC, Droplet Measurement Technologies), a high-resolution time-of-flight aerosol mass spectrometer (AMS, Aerodyne Research), and a scanning mobility particle sizer (SMPS, DMA3: models 3080 and 3081, TSI, CPC3: model 3025A, TSI). Prior to the analysis using the HTDMA-CCNC system, the aerosol was dried (reading of RH $<1\%$) in two diffusion driers, one with silica gel and the other with a molecular sieve (13X/4A mixture, Spelco and Sigma-Aldrich). After the aerosol was passed through the impactor and neutralizer (^{241}Am, 3 MBq), particles with a specific dry mobility diameter ($d_{p,dry}$, from 24.1 to 359 nm) were selected in the first DMA (DMA1, Model 3081, TSI) of the HTDMA. The classified aerosol was then humidified in Nafion tubing (MD110-24S-4, Perma Pure LLC) and was introduced into the second DMA (DMA2, Models 3080 and 3081, TSI) and a condensation particle counter (CPC1, Model 3775, TSI). The size distribution of the aerosol was measured using DMA2 and CPC1 to obtain size-resolved g distributions at $85 \pm 1\%$ RH. The residence time in the sample line downstream of the humidifier and upstream of DMA2 was estimated to be 12 s.

Particles selected in DMA1 were also introduced into the CCNC and another condensation particle counter (CPC2, Model 3025A, TSI), and the size-resolved ratios of CCN to CN were measured under supersaturation (SS) conditions of 0.12%, 0.24%, and 0.43%. The time for one cycle of measurements of the g distributions and the ratios of CCN to CN was 3 h. The measurements were performed for 34 particle sizes in $d_{p,dry}$ ranging from 24.1 to 359 nm; the sets of $d_{p,dry}$ depend on the SS conditions. The ratios of the sheath to sample flow rates for the DMAs in the HTDMA and CCNC were 10:1. The sample flow rate of DMA1 in the HTDMA was 0.65 L min^{-1}. The sample flow rates of DMA2 in the HTDMA, the CCNC, and CPC2 were 0.3, 0.3, and 0.05 L min^{-1}, respectively. We confirmed that the sample flow exiting DMA1 in the HTDMA (upstream of the humidifier) was dried (reading of RH: $<1\%$) and that the sample and sheath flows entering DMA2 and the sheath flow exiting DMA2 in the HTDMA were conditioned to ~85% RH using temperature and humidity sensors (HMT 337, Vaisala).

In the sampling line for the AMS and the SMPS, aerosols were dried (reading of RH: <1%) by the passage of two diffusion driers as in the case of the HTDMA-CCNC line. Bulk and size-resolved mass concentrations of nonrefractory submicron components (NR-PM_1), i.e., organic matter (OM), sulfate, nitrate, ammonium, and chloride, were measured every 5 min in the MS and PToF modes (V mode) using the AMS (vaporizer temperature: ~600°C). The number-size distributions in the range of $d_{p,dry}$ from 14.1 to 735 nm ($dN_{CN}/d \log d_{p,dry}$) were measured every 5 min using the SMPS. The sample flow rates of the AMS and the SMPS were 0.3 and 0.3 L min^{-1}, respectively. The ratio of the sheath to sample flow rates of DMA3 in the SMPS was 10:1. The sheath flow exiting DMA3 in the SMPS was confirmed to be dried (reading of RH: <1%) using a sensor (HMT 337, Vaisala). We also confirmed that the excess flow at the inlet of the AMS was dried (reading of RH: <8%) using another sensor (TR77Ui, T&D).

The PM_1 aerosol in the second sampling line was introduced into an EC/OC analyzer (model 4, Sunset Laboratory) at a sample flow rate of 7.4 L min^{-1}. Mass concentrations of elemental carbon (EC) and organic carbon (OC) were obtained every 90 min using a modified version of the protocol from the National Institute for Occupational Safety and Health (NIOSH) [*Nakayama et al*., 2014].

A series of calibrations for instruments, the HTDMA, SMPS, CCNC, AMS, and EC/OC analyzer, were performed before and after atmospheric observations. Detailed information about the calibrations is presented in Text S2 of SI.

2.2. Data Processing

The hygroscopic growth factor g is defined as the ratio of the electrical mobility diameter under humidified conditions ($d_{p,wet}$) to that under dry condition ($d_{p,dry}$). Size-resolved g distributions of particle number concentrations, n (log $d_{p,dry}$, log g) at specific $d_{p,dry}$, were derived with an inversion calculation to correct for the widths of the transfer functions of the DMAs using the Twomey algorithm [*Mochida et al*., 2010]. In this case, the integral of n (log $d_{p,dry}$, log g) along the log g axis at a fixed diameter corresponds to the SMPS-derived $dN_{CN}/d \log d_{p,dry}$ at the specified diameter. For atmospheric aerosol particles, the mean g for g distributions measured every 3 h for respective $d_{p,dry}$, g_m and the average g that corresponds to the mean volume of water retained by particles, g_{m_water}, were calculated by the following equations:

$$g_m = \frac{\sum n(\log d_{p,dry}, \log g) \bullet g}{\sum n(\log d_{p,dry}, \log g)} \quad (0.8 \le g \le 2.2) \tag{1}$$

$$g_{m\_water} = \left[\left(\frac{\sum n(\log d_{p,dry}, \log g) \bullet (g^3 - 1)}{\sum n(\log d_{p,dry}, \log g)} \right) + 1 \right]^{\frac{1}{3}} \quad (0.8 \le g \le 2.2) \tag{2}$$

For g distributions measured every 3 h for respective $d_{p,dry}$, mean values for the ranges of $0.8 \le g \le 1.1$ and $1.1 \le g \le 2.2$ (g_l and g_h, respectively) were also calculated.

The CCN efficiency spectra (the size-resolved ratios of CCN to CN) of singly charged particles were derived with corrections for diffusion losses in the sampling line, the presence of multiply charged particles, and the width of transfer functions [*Mochida et al*., 2010, 2011; *Kawana et al*., 2014]. The CCN activation parameters, F_{act}, d_{act}, and σ were derived by fitting using the equation proposed by *Rose et al*. [2008];

$$f_{fit} = \frac{F_{act}}{2} \left[1 + \mathrm{erf} \left(\frac{d_{p,dry} - d_{act}}{\sigma \sqrt{2}} \right) \right] \tag{3}$$

Here F_{act} is the value that f_{fit} approaches as $d_{p,dry}$ increases, and σ is the standard deviation (SD). In this study, a fitting using equation (3) was performed considering broadening because of the widths of transfer functions of DMA1 using the Matlab program (Mathworks, version R2008a). This fitting is to find F_{act}, d_{act}, and σ that lead Q in the following equation to be minimum.

$$Q = \sum_i \left[R_{meas} - \int f_{fit}(\log d_{p,dry}) \left(\frac{dn_{1+}}{d \log d_{p,dry}} \right) \Omega_i (\log d_{p,dry}) d \log d_{p,dry} \Big/ \int \left(\frac{dn_{1+}}{d \log d_{p,dry}} \right) \Omega_i (\log d_{p,dry}) d \log d_{p,dry} \right]^2 \tag{4}$$

where R_{meas} is the measured number fraction of CCN using the CCNC and CPC2 with the ith size setting of DMA1 but with correction for multiply charged particles [*Mochida et al*., 2010], f_{fit} (log $d_{p,dry}$) is f_{fit} represented

as a function of log $d_{p,dry}$, dn_{1+}/d log $d_{p,dry}$ is the hypothetical number-size distribution of +1 charged particles entering the CCNC and CPC2 if all +1 charged particles fully pass through DMA1 regardless of size, and Ω_i ($d_{p,dry}$) is the transfer function of DMA1 with the *i*th size setting [*Stolzenburg*, 1988].

2.3. Calculation of Hygroscopicity Parameter κ

To evaluate the hygroscopicity of particles and chemical components, the hygroscopicity parameter κ [*Petters and Kreidenweis*, 2007] was derived from both HTDMA and CCNC measurements. The κ value relates the saturation ratio of water vapor (S) in equilibrium with the droplet surface to the droplet diameter:

$$S = \frac{{d_{p,wet}}^3 - {d_{p,dry}}^3}{{d_{p,wet}}^3 - {d_{p,dry}}^3(1-\kappa)} \exp\left(\frac{4\sigma_s M_w}{RT\rho_w d_{p,wet}}\right) \quad (5)$$

Here σ_s is the surface tension, M_w is the molecular weight of water, R is the universal gas constant, T is the absolute temperature, and ρ_w is the density of water.

The κ values of particles under subsaturated conditions were calculated from the size-resolved g at 85% RH, which were obtained using the HTDMA. These HTDMA-based κ (κ_{HTDMA}) values were calculated using the following equation, which can be derived by the rearrangement of equation (5) with an S value of 0.85 (85%):

$$\kappa_{HTDMA} = \left(g^3 - 1\right)\left[\frac{\exp\left(\frac{4\sigma_s M_w}{RT\rho_w d_{p,wet}}\right)}{0.85} - 1\right] \quad (6)$$

For the calculation, T was assumed to be 301 K, the mean temperature of the sheath flow exiting DMA2 during observation. The σ_s value was assumed to be identical to that of pure water and was calculated with consideration of the temperature dependence [*Hänel*, 1976].

Furthermore, the κ values of particles under supersaturated conditions (κ_{CCNC}) were calculated from the measurement using the CCNC. The κ_{CCNC} value was computed using equation (5). In the calculation, with the CCN activation diameter d_{act} as an input of $d_{p,dry}$, the maximum value of S in equation (5) (s_c) was calculated using a solver for respective κ values that were increased from 0.1 in increments of 0.001. The κ value in the case in which ($s_c - 1$) is closest to the SS condition in the CCNC was then used as κ_{CCNC}. T was assumed to be 302 K, the mean temperature of the top of the column of the CCNC during observation. The σ_s value was assumed as in the calculation of κ_{HTDMA}.

For the analyses conducted in this study, the κ values of ammonium sulfate and ammonium nitrate under subsaturated conditions (κ_{AS} and κ_{AN}, respectively) and supersaturated conditions (κ_{AS_SS} and κ_{AN_SS}, respectively) were calculated. For the calculation of κ_{AS} and κ_{AN}, the g values of ammonium sulfate and ammonium nitrate at 85% RH were calculated from the Köhler model incorporating the Pitzer equation [*Pitzer and Mayorga*, 1973] and the molality-based surface tension [*Hänel*, 1976]. The κ_{AS} and κ_{AN} values were then obtained from equation (6) (with substitution of κ_{HTDMA} with κ_{AS} or κ_{AN}), with the σ_s value of pure water based on *Hänel* [1976]. The temperature assumed to calculate κ_{AS} and κ_{AN} was 301 K. In addition, the κ_{AS_SS} and κ_{AN_SS} values were calculated in the same manner as κ_{CCNC} but using the Köhler equation with the Pitzer equation and the molality-based surface tension [*Hänel*, 1976] instead of equation (5). The temperature assumed to calculate κ_{AS_SS} and κ_{AN_SS} was 302 K.

2.4. Calculation of Hygroscopicity Parameter κ for Organics

The hygroscopicity parameter of organics (κ_{org}) was calculated from the hygroscopicity parameter of particles at 85% RH (κ_{HTDMA}) and their chemical composition. The κ values of organics derived from κ_{CCNC} are discussed but are presented in Appendix A. The κ_{org} values were calculated by two different methods. One method is based on the extrapolation of the regression line of κ_{HTDMA} versus the volume fractions of organics (ε_{org}) [*Meng et al.*, 2014] (hereafter referred to as the regression method). The other is based on the analysis of the hygroscopicity parameters and volume fractions of the individual components with the Zdanovskii-Stokes-Robinson (ZSR) mixing rule [*Petters and Kreidenweis*, 2007; *Mei et al.*, 2013a, 2013b] (hereafter referred to as the ZSR-individual method). In both methods, particles were assumed to consist of organics, inorganic salts (ammonium sulfate and ammonium nitrate), and EC based on the results obtained from the AMS and EC/OC analyzer. From the calculations, size-resolved κ_{org} values at $d_{p,dry}$ of 60, 100, 200,

and 359 nm were derived. The averages of κ_{HTDMA} over the ranges of 50–71, 85–122, 175–250, and 300–359 nm were considered to be κ_{HTDMA} at 60 nm, 100 nm, 200 nm, and 359 nm, respectively. The compositions over the ranges of 65–93, 101–172, 209–350, and 363–624 nm in d_{va} were considered to be those at 60 nm, 100 nm, 200 nm, and 359 nm in $d_{p,dry}$, respectively, based on the equation proposed by *Decarlo et al.* [2004]. The ranges of d_{va} correspond to the cases in which spherical particles without voids have densities ranging from ~1.0 to ~1.8 g cm^{-3}. Additionally, size-averaged κ_{org} values were obtained by using all data at four $d_{p,dry}$. The volume fractions of organics, ammonium sulfate, ammonium nitrate, and EC (ε_{org}, ε_{AS}, ε_{AN}, and ε_{EC}, respectively) were calculated based on the assumptions of the densities of organics and inorganic salts detailed in Text S3 of SI and assuming a density of 2.0 g cm^{-3} for EC. The ε_{EC} value was calculated from the mass fraction of EC in total submicrometer aerosol mass concentrations as defined by the sum of NR-PM$_1$ and EC. Note that a regression method based on the κ value of particles versus the mass fractions of organics [*Shinozuka et al.*, 2009; *Gunthe et al.*, 2011] was not used. This is because the difference in density between organics and inorganics leads to a nonlinear theoretical mixing line with the ZSR assumption, suggesting the introduction of a bias into κ_{org}.

In the ZSR-individual method, the κ_{org} value was calculated using ε_{org} [*Mei et al.*, 2013a, 2013b] for every 3 h:

$$\kappa_{org} = \frac{\kappa_{HTDMA} - \left(\kappa_{AS}\varepsilon_{AS} + \kappa_{AN}\varepsilon_{AN} + \kappa_{EC}\varepsilon_{EC}\right)}{\varepsilon_{org}} \tag{7}$$

where κ_{org}, κ_{AS}, κ_{AN}, and κ_{EC} are the hygroscopicity parameters of organics, ammonium sulfate, ammonium nitrate, and EC. The κ_{EC} value was assumed to be zero.

2.5. CCN Closure

The ratios of N_{CCN} to the total number concentrations of aerosol particles (N_{CN}) at $d_{p,dry}$ ranging from 24 to 359 nm were predicted using data from the SMPS and the HTDMA (and also the AMS data in some cases) and were compared with values measured from the SMPS data coupled with the CCNC and CPC2 data. This comparison was made to investigate the effects of the variations in g with size and time, g distributions, and the hygroscopicity of organics on the number fraction of CCN. The N_{CN} for both predicted and measured N_{CCN}/N_{CN} were obtained from the SMPS. In the derivation of the measured N_{CCN}, the ratios of CCN to CN obtained at respective $d_{p,dry}$ using the CCNC (different sets of 34 diameters for each SS, with the correction for multiply charged particles) were used as the CCN number fractions at the corresponding bins of the SMPS size bins (76 bins for 24–359 nm). For the other SMPS size bins, the ratios at the midpoint diameter of the bins on the logarithmic scale were estimated by linear interpolation and were used for the bins. The N_{CCN} values in the range of 24–359 nm were then calculated based on the SMPS-derived number-size distributions and the CCN/CN ratios at respective bins.

The prediction of N_{CCN} to assess the effects of the hygroscopicity distributions was based on the distributions of g for each SMPS size bin in the range from 24 to 359 nm. For the size bins in which the HTDMA-derived g distributions were obtained, the measured distributions were applied. For the other bins, the distributions were assumed so that the probability density functions of g were identical to those in the nearest bins at which g distributions were measured and that the integration of the distributions along the axis of log g was equal to dN_{CN}/d log $d_{p,dry}$ from the SMPS. In considering (1a) time- and size-resolved g distributions, the κ values of particles in each bin of g and $d_{p,dry}$ (resolutions of g and $d_{p,dry}$: 64 bins per decade) were calculated using equation (6). Particles in each bin were considered as CCN if the maximum values of S in equation (5) with the derived κ values were lower than the saturation ratio in the CCNC. The sum of the CCN concentration in each $g - d_{p,dry}$ bin is the predicted N_{CCN} value over the range from 24 to 359 nm. For this case, the g values every 3 h were used. Prediction of N_{CCN} were also performed by applying simplification(s) to case 1a: (2a) time- and size-resolved g, (3a) time-averaged and size-resolved g, (4a) time-resolved bulk g, and (5a) a constant mean bulk g throughout the observation period. The g values for case 2a were obtained using equation (2), and the time-averaged value at respective $d_{p,dry}$ was used in case 3a. The time-resolved bulk g in case 4a corresponds to the average of g in terms of the volume of retained water relative to that of solute over d_{act} values ranging from 24.1 to 359 nm:

$$g_{m\_water\_avg} = \left[\left(\frac{\sum_{\log dp,dry}\sum_{\log g} n(\log d_{p,dry}, \log g) \bullet (g^3 - 1)}{\sum_{\log dp,dry}\sum_{\log g} n(\log d_{p,dry}, \log g)}\right) + 1\right]^{\frac{1}{3}} \tag{8}$$

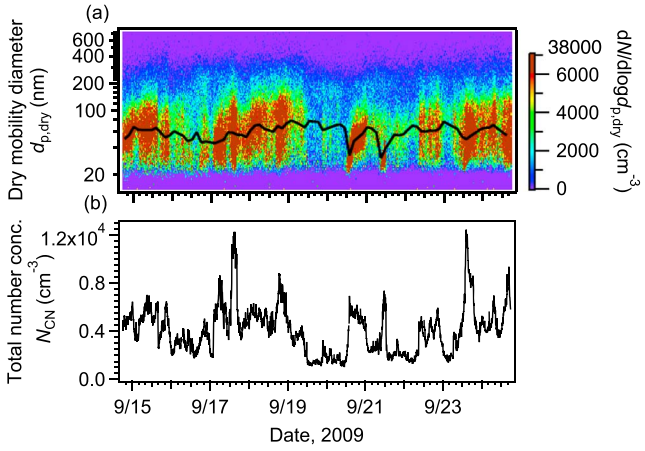

Figure 2. Time series of (a) the number-size distributions and (b) the total number concentrations of aerosol particles (N_{CN}) in the size range of 14.1–735 nm. The black line in Figure 2a represents the mode diameters of fitted single lognormal functions.

The constant mean bulk g of 1.27 in case 5a is the time average of the time-resolved bulk g in case 4a. In cases 2a–5a, the derived g values were applied to the particles at different $d_{p,dry}$ at different times, and the number concentrations of particles that act as CCN were determined as in case 1a.

The N_{CCN} values over the range from 24 to 359 nm were also predicted with different assumptions of the hygroscopicity of organics (κ_{org}), i.e., (1b) κ_{org} values corresponding to particles at d_{act} under three SS conditions (section 3.3), (2b) the average of the three κ_{org} values used in case 1b, and (3b) the assumed κ_{org} values based on the literature (0, 0.1, and 0.2). For cases 1b and 2b, the size-resolved and size-averaged κ_{org} values for each 3 h measurement period were used, respectively. In the analysis, the κ values of particles were calculated by the ZSR-individual approach using the assumed or obtained κ_{org}, with κ_{AS}, κ_{AN}, κ_{EC}, ε_{AS}, ε_{AN}, ε_{EC}, and ε_{org} used for the calculations of size-resolved (or size-averaged) κ_{org} for each 3 h period (section 2.4). The corresponding CCN activation diameters were then estimated, and particles larger than the activation diameters among those with the SMPS-derived size distributions were regarded as CCN.

3. Results and Discussion

3.1. Number-Size Distributions and Chemical Composition

The time series of the number-size distributions of aerosol particles is presented in Figure 2a. In the figure, the particles in the Aitken mode range ($d_{p,dry} < 100$ nm) were dominant (mean: 76%) among total particles in the range of 14.1–735 nm. The mode diameters derived from fittings with a single lognormal curve are also presented in Figure 2a. The mean ± SD of the mode diameters was 59 ± 10 nm. The time series of N_{CN} is depicted in Figure 2b. The mean ± SD of N_{CN} was 4101 ± 1983 cm^{-3}. The increase in N_{CN} accompanying a small-mode diameter (~30 nm) around noon and subsequent increases in the mode diameter in the afternoon were observed on 20 and 21 September. This phenomenon can be explained by the occurrence of new particle formation [*Salma et al.*, 2011; *Ahlm et al.*, 2012] and/or the primary emission of particles such as HOA particles [*Zhang et al.*, 2005a, 2005b], followed by their growth caused by coagulation and condensation.

The time series of the mass concentrations of chemical components in AMS and carbonaceous components is presented in Figures 3a and 3b. The mean ± SD of the mass concentrations of the sum of NR-PM$_1$ components (OM, sulfate, ammonium, nitrate, and chloride) and EC was 8.1 ± 3.5 μg m^{-3}. The time series of the mass fractions is shown in Figure 3c. The mean ± SD of the mass fractions of OM, sulfate, ammonium, nitrate, chloride, and EC among these components were 53% ± 9%, 23% ± 8%, 10% ± 2%, 7% ± 5%, 0.1% ± 0.1%, and 8% ± 4%, respectively. As observed at other urban sites, organics were dominant [*Zhang et al.*, 2007; *Jimenez et al.*, 2009]. The time series of the ratios of OM/OC, O/C, and H/C are presented in the SI (Figure S4b). The mean ± SD of OM/OC, O/C, and H/C were 1.62 ± 0.09, 0.37 ± 0.07, and 1.56 ± 0.08, respectively. The mean value of OM/OC was similar to values proposed in previous studies: 1.6 (in urban areas) to 2.1 (in nonurban areas) [*Turpin and Lim*, 2001; *Pang et al.*, 2006]. Note that the uncertainties in the mass concentrations of chemical components are discussed in the SI (see Text S3 and Figures S3 and S4).

The average mass-size distributions of NR-PM$_1$ components are presented in Figure 3d. The mass fraction of organics was relatively large at small diameters, and the mass fraction of inorganics tended to be larger at larger diameters. The mass and volume fractions of particles, f_{43}, f_{44}, and f_{57} (the ratios of the signal intensities at m/z 43, 44, and 57, respectively, to those of total organic aerosol) in different size ranges are summarized in

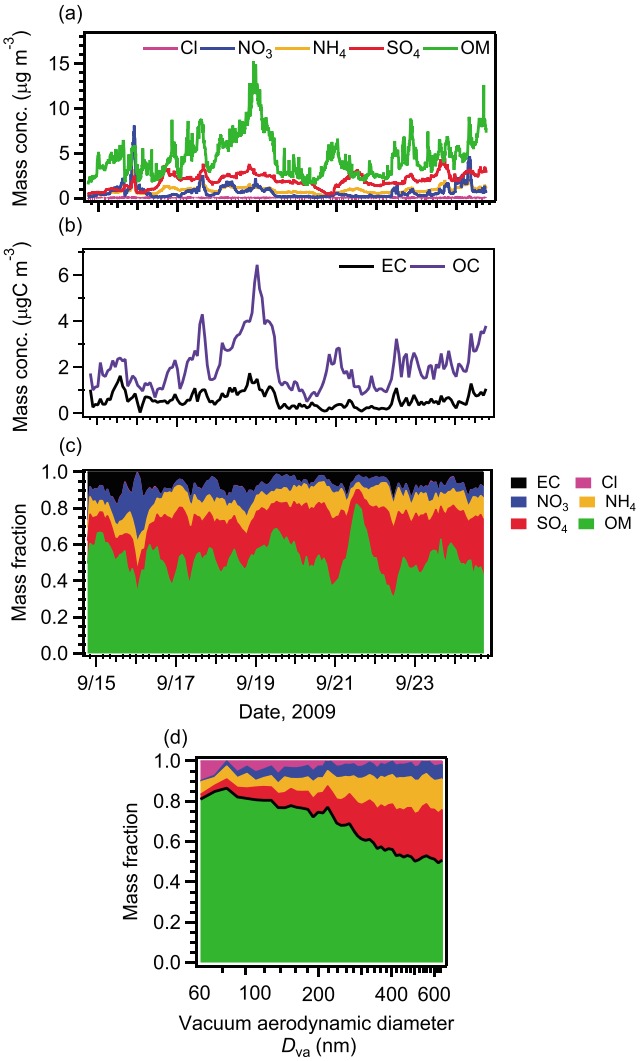

Figure 3. Time series of (a) the mass concentrations of nonrefractory submicron ($NR\text{-}PM_1$) components, (b) the mass concentrations of EC and OC, and (c) the mass fractions of $NR\text{-}PM_1$ components and EC. (d) The mass fractions obtained from the average of the size-resolved mass distributions of $NR\text{-}PM_1$ components.

Table S1 of the SI. The f_{57} and f_{44} are associated, respectively, with HOA and oxygenated organic aerosol (OOA), and the f_{43} is associated with HOA and the less-oxygenated semivolatile OOA (SV-OOA) fraction of the OOA [*Ng et al.*, 2010]. The smaller the diameter were, the larger f_{57} and f_{43} became, and an opposite size dependence was observed for f_{44}. The result indicates that the mass fraction of less-oxygenated organics was relatively large in the Aitken mode range and that the fraction of highly oxygenated OOA (as well as nitrate and sulfate as presented in Figure 3c) was relatively large in the accumulation mode range. This size dependence of the chemical components is in line with the size dependence in the previous reports [*Zhang et al.*, 2005a, 2005b; *Takegawa et al.*, 2006].

3.2. Size-Resolved Distribution of Hygroscopic Growth Factors

The time series of the g distributions at 49.6, 102, 209, and 300 nm as examples are presented in Figure 4. The size-resolved mean g values for $0.8 \le g \le 2.2$, $0.8 \le g < 1.1$, and $1.1 \le g \le 2.2$ (g_m, g_l, and g_h, respectively) are also presented. The distributions of g at both small (49.6, 102 nm) and large (209, 300 nm) diameters generally showed bimodal characteristics, indicating the externally mixed conditions of the aerosols. Bimodal g distributions, as observed in this study, have commonly been observed in urban environments [*McFiggans et al.*, 2006; *Massling et al.*, 2009]. The size-resolved mean g values and other parameters related to particle hygroscopicity for selected eight dry diameters are summarized in Table 1. The average of two-dimensional g distributions with axes of $d_{p,dry}$ and g ($d_{p,dry}$: 24.1–359 nm, $0.8 \le g \le 2.2$) and that normalized are presented in Figures 5. The average distribution of g was bimodal and had less and more hygroscopic modes. However, the two-dimensional g distributions did not always show clearly bimodal characteristics (Figures S5 and S6 in the SI), as also shown in Figure 5.

As presented in Table 1, g_m tended to be larger at larger diameters. The g_h values were substantially size dependent, similar to g_m, whereas g_l values were not. The g_m values at eight sizes in Table 1 all correlate substantially with g_h (r: 0.55–0.92), whereas the correlations with g_l were weakly negative (r: −0.07 to −0.23); this result indicates that the temporal variations in the g distributions of more hygroscopic particles ($1.1 \le g \le 2.2$) contributed more strongly to the variation of g_m than those of less hygroscopic particles. The variations in the number fractions of more hygroscopic particles should also contribute to the variation in g_m, as suggested by the correlation between g_m and the fractions at eight sizes in Table 1 (r: 0.66–0.89). The mean ± SD of g_m at respective diameters ranging from 24 to 359 nm at 16 sizes were 1.27 ± 0.08. The

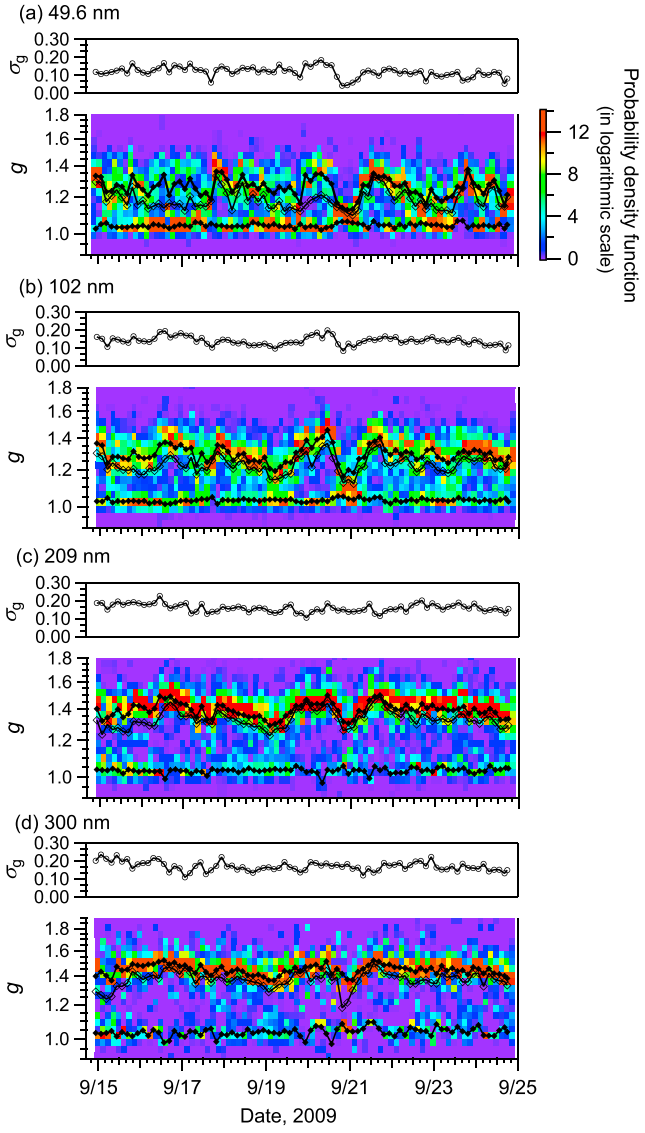

Figure 4. Time series of g distributions and the standard deviation σ_g at 85% RH for $d_{p,dry}$ of (a) 49.6 nm, (b) 102 nm, (c) 209 nm, and (d) 300 nm. Open and solid symbols represent the mean g values in the range of $0.8 \le g \le 2.2$ and those in the ranges of $0.8 \le g < 1.1$ and $1.1 \le g \le 2.2$, respectively.

g_{m_water} and κ_{HTDMA} values calculated from equation (6) with g_{m_water} as an input of g also showed increasing trends with the increase in diameter.

The mean ± SD of κ_{HTDMA} at respective diameters, where κ_{HTDMA} was calculated from g_{m_water} at 16 sizes, were 0.22 ± 0.06. The mean κ_{HTDMA} (0.22) in this study is within the range of κ obtained from several other observations (0.3 ± 0.1) [*Andreae and Rosenfeld*, 2008] and from a model calculation (0.27 ± 0.21 under supersaturated condition) [*Pringle et al.*, 2010] for continental sites. Furthermore, the value is similar to the κ of Asian continental aerosols obtained from a model calculation (0.22 ± 0.15 under supersaturated conditions) [*Pringle et al.*, 2010] and from some observations at urban sites (0.12–0.27 using HTDMA) [*Jurányi et al.*, 2013]. Although comparisons should be made with caution because κ values under subsaturated and supersaturated conditions should not be identical, the above mentioned comparison shows that the mean κ obtained in this study is close to that reported for urban and continental aerosols in the literature.

The number-size distributions and number fractions of particles in four different ranges of g are presented in Figure 6. In the Aitken mode range, particles in the range of $0.8 \le g < 1.25$ were dominant (mean : 65%). By contrast, in the accumulation mode range, particles in the range of $1.25 \le g < 2.2$ were dominant (mean : 70%). A similar characteristic was reported for Beijing: The number fractions of more hygroscopic particles (g at 90% RH: 1.26–1.62) at a large diameter range were relatively larger than those in a smaller diameter range [*Massling et al.*, 2009]. The dominance of particles with relatively low hygroscopicity ($0.8 \le g < 1.25$) in the small diameter range and that of relatively high hygroscopicity ($1.25 \le g < 2.2$) in the large diameter range are explained by their chemical composition, sources, and aging processes. The size-resolved chemical composition in Figure 3 and characteristics of size-resolved hygroscopicity in Figures 4–6 suggest that Aitken mode particles mainly consisted of locally emitted fresh HOA with low hygroscopicity and that accumulation mode particles mainly consisted of inorganic salts and OOA with high hygroscopicity. Additionally, locally emitted fresh black carbon (BC) might be regarded as a part of particles with relatively low hygroscopicity. The above mentioned assignment is similar to that of *Massling et al.* [2009], who reported that high number fractions of nearly hydrophobic (g at 90% RH: 0.96–1.07) and less hygroscopic particles (g : 1.06–1.29) in the Aitken mode indicate high amounts of carbonaceous materials. Furthermore, the assignment is also similar to that of *Mochida et al.* [2008], who reported that particles with $g < 1.11$ were associated with primary compounds and that particles with $g > 1.29$ were associated with secondary or oxidized compounds based on an

Table 1. Values Associated With the Hygroscopicity of Aerosol Particles at 85% RH[a]

$d_{p,dry}$ (nm)	g_m[b]	g_l[c]	g_h[d]	σ_g[e]	g_{m_water}[f]	κ_{HTDMA}[g]
28.9	1.17 ± 0.05	1.05 ± 0.02	1.25 ± 0.05	0.11 ± 0.03	1.18 ± 0.05	0.17 ± 0.03
49.6	1.19 ± 0.06	1.04 ± 0.01	1.26 ± 0.06	0.12 ± 0.03	1.20 ± 0.06	0.17 ± 0.03
71	1.21 ± 0.06	1.04 ± 0.01	1.27 ± 0.06	0.13 ± 0.03	1.22 ± 0.06	0.17 ± 0.03
102	1.24 ± 0.05	1.03 ± 0.01	1.30 ± 0.06	0.14 ± 0.02	1.26 ± 0.06	0.19 ± 0.02
146	1.29 ± 0.06	1.03 ± 0.01	1.35 ± 0.06	0.15 ± 0.02	1.31 ± 0.06	0.24 ± 0.03
209	1.34 ± 0.06	1.03 ± 0.01	1.40 ± 0.05	0.16 ± 0.02	1.36 ± 0.05	0.28 ± 0.03
300	1.38 ± 0.06	1.04 ± 0.02	1.45 ± 0.04	0.17 ± 0.03	1.40 ± 0.05	0.32 ± 0.03
359	1.39 ± 0.07	1.03 ± 0.04	1.47 ± 0.04	0.18 ± 0.04	1.41 ± 0.05	0.33 ± 0.03

[a]Mean ± SD.
[b]Mean hygroscopic growth factors for particles in the range of $0.8 \le g \le 2.2$.
[c]Same as b but for particles in the range of $0.8 \le g < 1.1$.
[d]Same as b but for particles in the range of $1.1 \le g \le 2.2$.
[e]Standard deviation of g distributions in the range of $0.8 \le g \le 2.2$.
[f]Average hygroscopic growth factors from equation (2).
[g]The hygroscopicity parameter calculated from g_{m_water}.

observation made in the summer in Tokyo. Note that the g values of small particles were affected by the curvature effect (Kelvin effect) relatively more strongly (see the contour lines of κ_{HTDMA} in Figure 5), which may also contribute to the size dependence of g distributions in Figure 6. Whereas intermediately hygroscopic particles ($1.25 \le g < 1.4$) in addition to less hygroscopic particles ($g < 1.25$) were dominant in the Aitken mode range in Nagoya in summer 2010 [*Kawana et al.*, 2014], the fraction of intermediately hygroscopic particles was small in this study (0.85, 0.85, and 0.91 times at 30, 50, and 71 nm). In summer 2010, aged hygroscopic particles and maritime aerosol particles may have been substantially transported to the observation site because air mass trajectories originated mainly from China and the Pacific Ocean. By contrast, the contribution of such particles may have been relatively small in this study because the observed site was influenced by air masses originating mainly from surrounding areas in Japan (Figure S2).

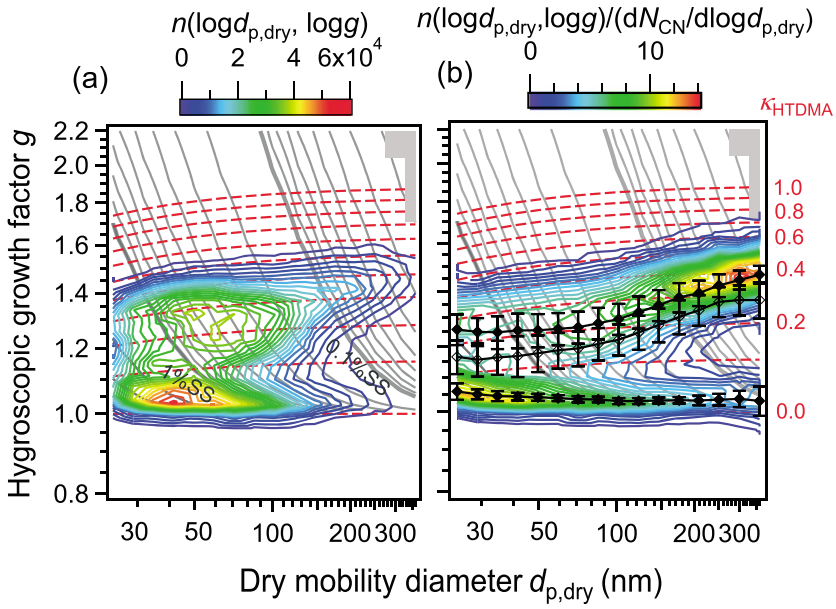

Figure 5. The averages of (a) two-dimensional distributions of the number concentrations of aerosol particles as a function of hygroscopic growth factors (g) and dry mobility diameter ($d_{p,dry}$) at 85% RH and (b) the distributions normalized by $dN_{CN}/d\log g$. The open and solid symbols in Figure 4b represent the mean values of g in the range of $0.8 \le g \le 2.2$ and those in the ranges of $0.8 \le g < 1.1$ and $1.1 \le g \le 2.2$ at 24.1–359 nm, respectively. The bars represent the standard deviations. The dashed red lines represent contours of κ_{HTDMA} at 85% RH. The gray contours show the critical SS estimated by the κ-Köhler theory [*Mochida et al.*, 2011].

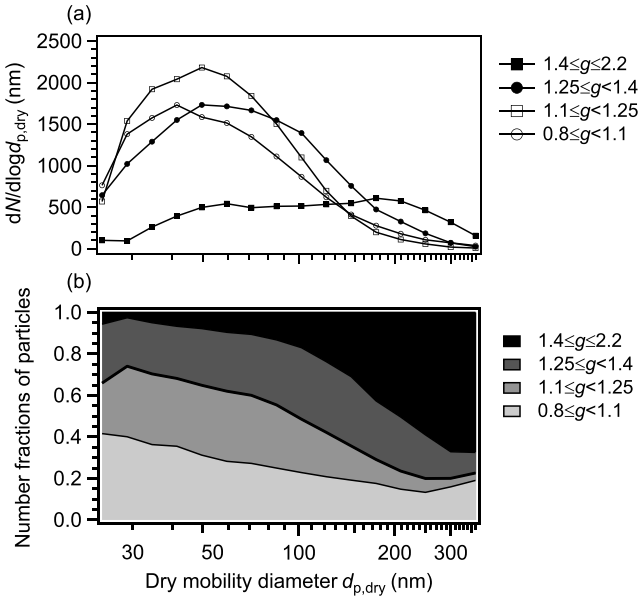

Figure 6. (a) The averages of the number-size distributions and (b) the number fractions derived from the averages of the number-size distributions of aerosol particles in the ranges of $0.8 \le g < 1.1$, $1.1 \le g < 1.25$, $1.25 \le g < 1.4$, and $1.4 \le g \le 2.2$.

3.3. Hygroscopicity Parameter of Organics and the Relation to the Oxidation State

The hygroscopicity parameter of organics (κ_{org}) was calculated by two different methods from the HTDMA-derived hygroscopicity of particles (κ_{HTDMA}) and the chemical composition. The regressions of κ_{HTDMA} versus ε_{org} are depicted in Figure 7a. The calculated κ_{org}, the values of the regression lines at ε_{org} of unity, are summarized in Table 2. The size-resolved κ_{org} values determined by the regression method were 0.12–0.18 (r: 0.58–0.78). The size-averaged κ_{org} values determined by a single regression line for data from all four $d_{p,dry}$ were 0.143 ($r = 0.81$). The κ_{org} values determined by the ZSR-individual method (Figure 7b) for 60–359 nm were 0.14–0.23. The size-averaged κ_{org} value, represented by the mean of κ_{org} at all four $d_{p,dry}$, was 0.188. The calculated mean κ_{org} values were relatively low in small particles and relatively high in large particles according to the calculations made using the two methods: 0.12–0.15 for 60 and 100 nm particles and 0.17–0.22 for 200 and 359 nm particles. The mean κ_{org} values determined by the two methods, 0.14 and 0.19, suggest that the organics were moderately hygroscopic nature. The values are similar to those reported for aerosols in Hong Kong (0.10–0.16, calculated from the average g of organics at 90% RH) [*Yeung et al.*, 2014] and for aerosols over Mexico City (0.13–0.21) [*Shinozuka et al.*, 2009] and are higher those reported for urban aerosols in Beijing (0.06) [*Gunthe et al.*, 2011] and near Guangzhou (0.10) [*Rose et al.*, 2011]. The higher values in Nagoya than those in Beijing and Guangzhou might have been caused by the effect of regionally transported aged organic aerosols from the Asian continent and other parts of Japan (Figure S2). Furthermore, the approximation of the relationship between the κ values of particles and the mass fraction of organics as a linear relationship in previous studies might have introduced some bias into κ_{org} (see also section 2.4). Note that a sensitivity analysis was performed for κ_{org}, with regard to the uncertainty of the mass fraction of EC and that of g (see section S4 in the SI for details). Doubling EC and fully ignoring it results in 8%–14% and 8%–14% changes in κ_{org}, respectively (temporal averages for 60, 100, 200, and 359 nm). If the percentage difference in the g values measured for pure ammonium sulfate particles from those calculated from literature values [*Tang and Munkelwitz*, 1994; *Hänel*, 1976] are regarded as the measurement bias of g, 6%–11% changes in κ_{org} (temporal averages for 60, 100, 200, and 359 nm) are obtained. These serve as guides for determining the uncertainty in κ_{org}.

The relationship of κ_{org} to f_{44} and O/C was investigated in previous studies [*Aiken et al.*, 2008; *Chang et al.*, 2010]. The regressions in this study resulted in the following equations: $\kappa_{org} = 1.300 \times f_{44} - 0.101$ and $\kappa_{org} = 0.193 \times \mathrm{O/C} - 0.070$ (Figures 7c and 7d). The κ_{org} versus f_{44} or O/C show positive but weak correlations ($r = 0.42$ and $r = 0.27$, respectively). Although the correlations were weaker than those reported in some studies [*Duplissy et al.*, 2011; *Mei et al.*, 2013a], the absence of strong correlations is not unique; weak correlations have also been reported in other studies [*Moore et al.*, 2011; *Lathem et al.*, 2013]. A fully quantitative comparison is not possible because the degrees of correlations might be affected by the uncertainty in κ_{org} and f_{44} or O/C and their variation ranges in respective studies. In this study, the uncertainty might in part be caused by the assumption of the volume fractions of EC at different sizes and the assumption of the size ranges of d_{va}. Furthermore, the O/C obtained from bulk composition data may weaken the correlation. Nevertheless, it is also possible that the hygroscopicity of organics and their degree of oxygenation is not simply represented by a linear positive correlation, as suggested in previous studies [*Rickards et al.*, 2013; *Yeung et al.*, 2014].

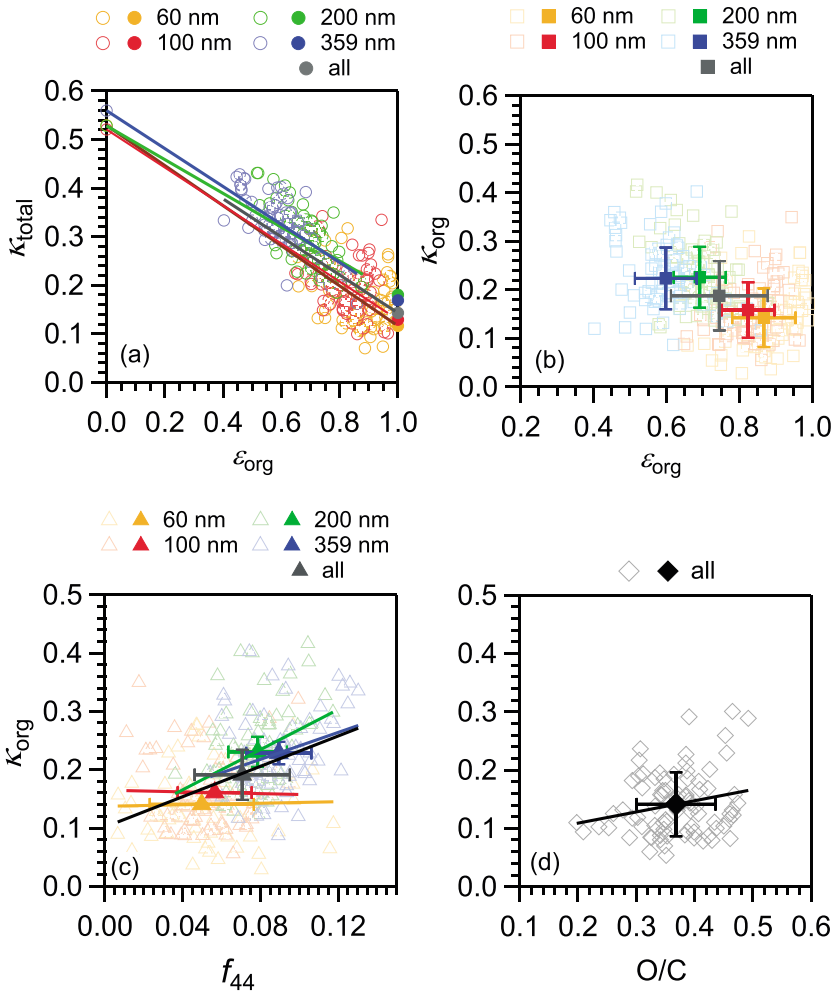

Figure 7. (a) Scatterplot of the HTDMA-derived hygroscopicity parameter (κ_{HTDMA}) versus organics volume fractions (ε_{org}). The solid squares represent size-resolved and size-averaged hygroscopicity parameters of organics (κ_{org}) obtained by the regression lines. (b–d) Scatterplot of Figure 7b κ_{org} obtained by the ZSR-individual method versus ε_{org}, Figure 7c ε_{org}-derived κ_{org} versus f_{44}, and Figure 7d ε_{org}-derived κ_{org} versus O/C. The solid lines in Figures 7a, 7c, and 7d represent the regression lines. Open symbols in Figures 7b and 7c represent individual values, and the solid symbols and bars represent the mean values of size-averaged (all) and size-resolved κ_{org} and the standard deviation, respectively.

3.4. CCN Activity

The time series of the size-resolved CCN activated fractions (F_{act}) and d_{act} at 0.12%, 0.24%, and 0.43% SS are presented in Figures 8a–8c. The parameters of CCN activation derived from fitted CCN efficiency spectra (F_{act}, d_{act}, and σ) and σ/d_{act}, a measure of the heterogeneity of aerosol particles [*Rose et al.*, 2008, 2010], are summarized in Figures 9a–9d and Table 3. The time series of F_{act}, d_{act}, and σ/d_{act} are also presented in Figures 8a–8c. The F_{act} values have a large mean (>0.9) and a small SD, indicating that fractions of CCN-inactive particles well above d_{act} were generally small. However, F_{act} values were low (<0.7) at the beginning of the observation period (on 14 September), indicating the substantial

Table 2. κ of Organics (κ_{org}) and the Correlation Coefficients

	κ_{org}	
d_{va} ($d_{p,dry}$) (nm)	Regression Method[a]	ZSR-Individual Method[b]
65–93 (60)	0.116 (0.61)	0.143 ± 0.060
101–172 (100)	0.129 (0.58)	0.159 ± 0.057
209–350 (200)	0.180 (0.75)	0.226 ± 0.063
363–624 (359)	0.169 (0.78)	0.223 ± 0.063
all[c]	0.143 (0.81)	0.188 ± 0.071

[a]Values in parentheses are correlation coefficients from the regression analysis.
[b]Mean ± SD.
[c]Values obtained by using all data points in four size ranges.

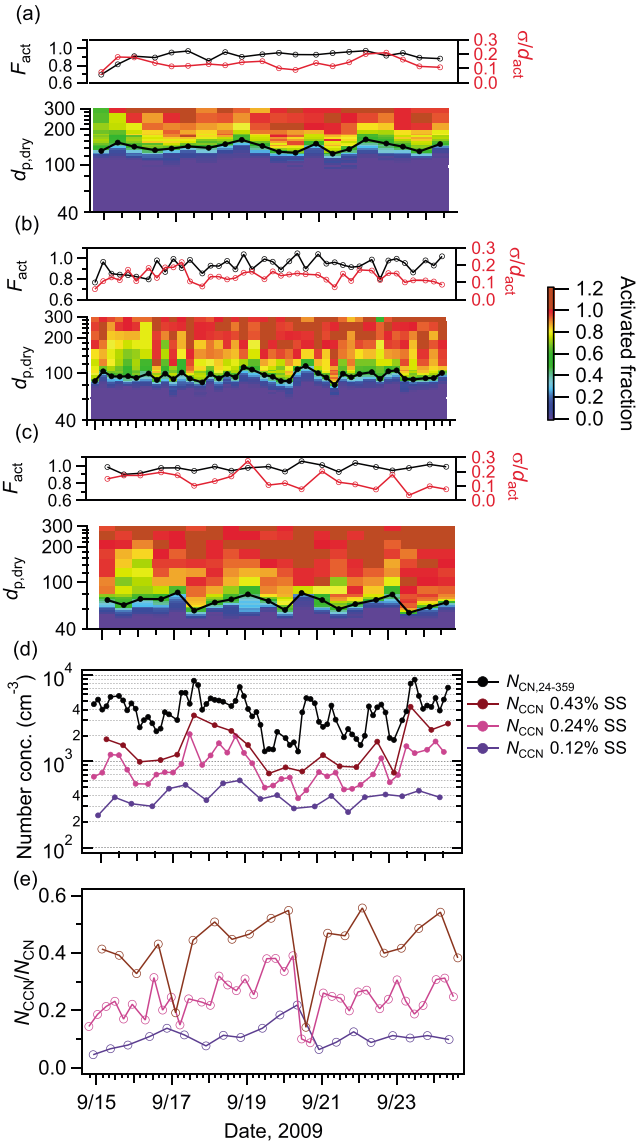

Figure 8. (a–c) Time series of size-resolved CCN activated fractions, F_{act}, and σ/d_{act} under (a) 0.12%, (b) 0.24%, and (c) 0.43% SS. (d) Time series of the number concentrations of CCN and CN from 24 to 359 nm (N_{CCN} and N_{CN}, respectively). (e) Time series of the ratios of N_{CCN} to N_{CN} under 0.12%, 0.24%, and 0.43% SS. Solid black circles in Figures 8a–8c represent CCN activation diameters d_{act}.

presence of CCN-inactive particles even well above d_{act}. The mass fraction of EC in this period was large (up to 30%) compared with the average (8%), suggesting that the presence of fresh soot particles resulted in low F_{act}. This finding is supported by the report of *Rose et al.* [2011], who suggested that CCN-inactive particles with large diameters (~300 nm) might be fresh soot particles based on the analysis of CCN activity and volatility for aerosols observed near a megacity in China. The above mentioned relationship regarding F_{act} also holds for the CCN fractions at the maximum diameter of 359 nm (F_{max}). The σ/d_{act} values averaged for the respective SS conditions were ~0.13, and the dependence on SS, and thus $d_{p,dry}$ (69–142 nm), was not evident. The σ/d_{act} values were substantially larger than the values of pure ammonium sulfate particles, i.e., particles composed of a single component (0.05, 0.03, and 0.02 at 112, 71, and 50 nm, respectively). This result suggests that ambient particles were inhomogeneous even for a specific size, as expected from g distributions (Figure 4). The σ/d_{act} correlated with the standard deviation of g, σ_g, over the range of $1.1 \leq g \leq 2.2$ (r: 0.52–0.60 at 0.12–0.43% SS), indicating that the nonuniformity of particle hygroscopicity is related to the CCN activity of particles. Figure 8 also shows the time series of N_{CN}, N_{CCN}, and N_{CCN}/N_{CN} over the range from 24 to 359 nm. The mean ± SD of N_{CCN} at 0.12%, 0.24%, and 0.43% were 391 ± 98, 925 ± 429, and 1676 ± 996 cm^{-3}, respectively. The mean ± SD of N_{CCN}/N_{CN} at 0.12%, 0.24%, and 0.43% were 0.11 ± 0.04, 0.24 ± 0.07, and 0.43 ± 0.11, respectively.

The values of F_{act}, d_{act}, σ, and σ/d_{act} obtained in this study are compared with those obtained in previous studies in Figure 9. The fitting parameters and derived values in this study are similar to those reported in previous studies [*Rose et al.*, 2010; *Gunthe et al.*, 2011; *Meng et al.*, 2014]. In the case of d_{act}, the dependence on SS suggests that the values obtained in this study were higher than those of aged particles in Asian remote sites [*Kuwata et al.*, 2008; *Mochida et al.*, 2010]. The κ_{CCNC} values calculated from d_{act} are presented in Figure 9e. The figure suggests that the smaller the particles are, the lower the hygroscopicity becomes, as in the case of κ_{HTDMA}. This trend has also been reported in previous studies. Although the trends of the κ_{CCNC} values obtained in this study were similar to those observed during the fresh city pollution period in the CAREBeijing campaign, they tended to be lower than those observed during the aged regional pollution period in the same campaign [*Gunthe et al.*, 2011].

The CCNC-derived κ values obtained under supersaturated conditions, κ_{CCNC}, were compared with the HTDMA-derived κ values obtained under subsaturated conditions, κ_{HTDMA} (Figure 10a and Table 3). In this

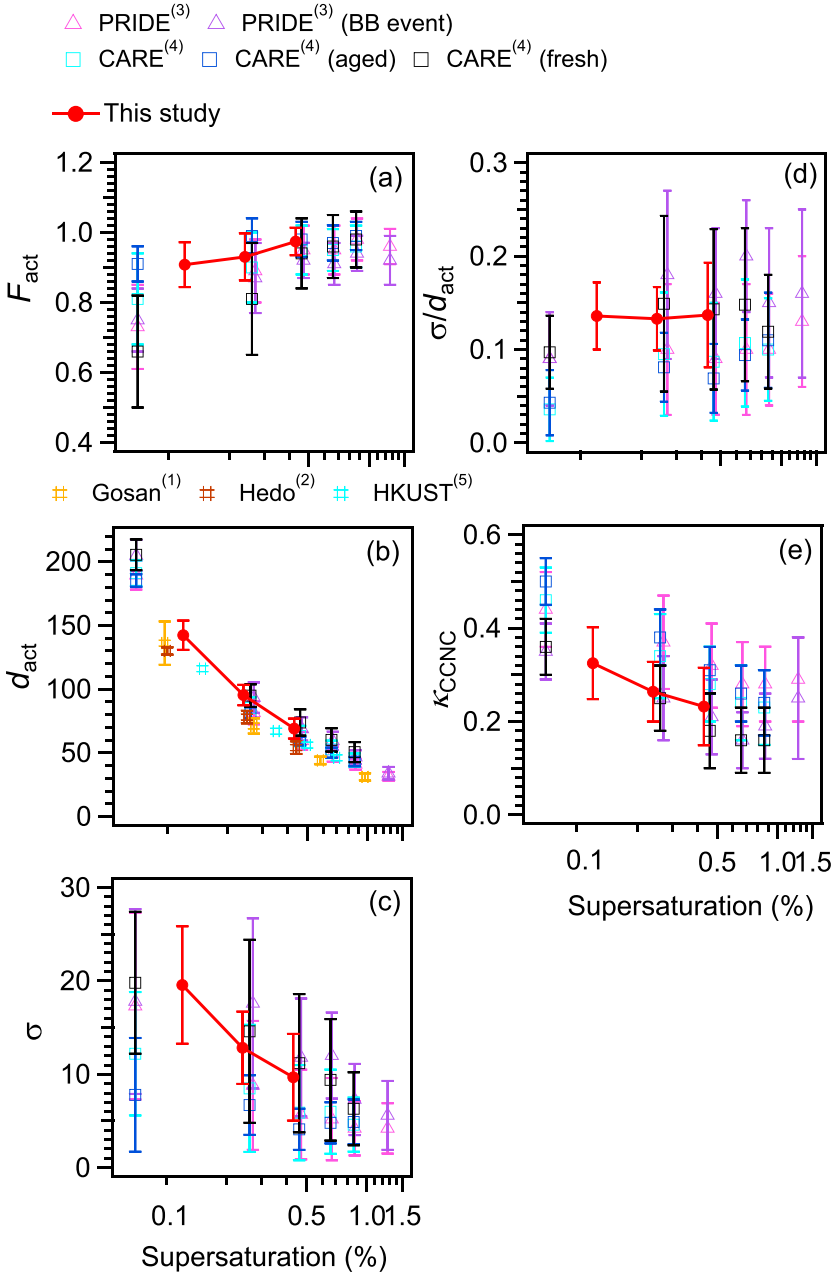

Figure 9. Parameters associated with CCN activation: (a) F_{act}, (b) d_{act}, (c) σ, (d) σ/d_{act}, and (e) κ_{CCNC}. Solid red circles and bars represent the mean values and the standard deviation, respectively. The figures also show the values reported by (1) *Kuwata et al.* [2008], (2) *Mochida et al.* [2010], (3) *Rose et al.* [2010], (4) *Gunthe et al.* [2011], and (5) *Meng et al.* [2014].

Table 3. Values Obtained by the Fitting of CCN Efficiency Spectra[a]

SS	F_{act}	F_{max}	d_{act}	σ	σ/d_{act}	κ_{CCNC}[b]	$\kappa_{CCNC}/\kappa_{HTDMA}$	$\kappa_{CCNC}/\kappa_{HTDMA}$*
0.12%	0.91 ± 0.06	1.01 ± 0.11	142.3 ± 11	19.6 ± 6.3	0.136 ± 0.040	0.324 ± 0.070	1.44 ± 0.13	1.27 ± 0.12
0.24%	0.93 ± 0.07	1.00 ± 0.11	95.3 ± 8	12.8 ± 3.9	0.133 ± 0.030	0.264 ± 0.060	1.39 ± 0.21	1.32 ± 0.18
0.43%	0.97 ± 0.04	1.04 ± 0.04	69.0 ± 8	9.7 ± 4.6	0.125 ± 0.070	0.232 ± 0.080	1.25 ± 0.14	1.21 ± 0.13
all[c]							1.37 ± 0.19	1.28 ± 0.16

[a]Mean ± SD.
[b]Hygroscopicity parameter calculated from d_{act}.
[c]Values obtained by using all data points at 0.12%, 0.23%, and 0.43% SS.

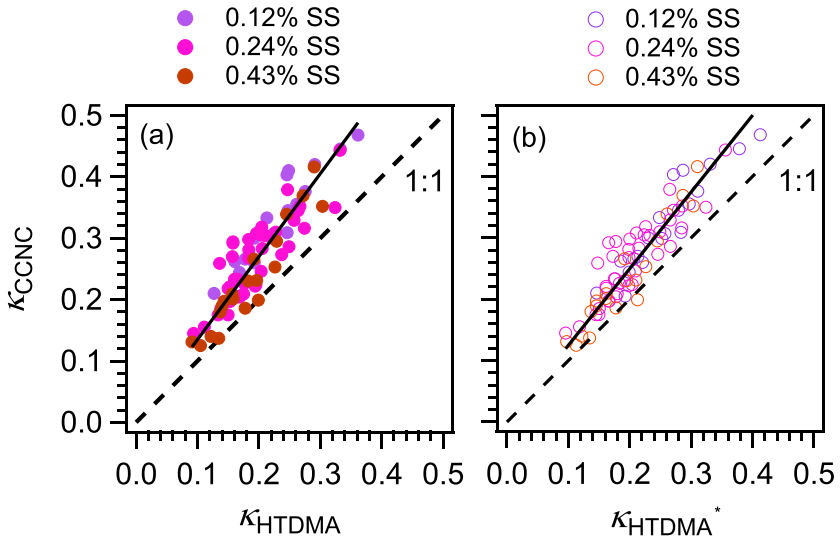

Figure 10. (a) Scatterplot of κ_{CCNC} versus κ_{HTDMA} under 0.12%, 0.24%, and 0.43% SS. Solid circles and the solid line represent κ_{CCNC} plotted against κ_{HTDMA} and the regression line constrained through the origin, respectively. (b) Scatterplot of κ_{CCNC} versus κ_{HTDMA}^{*} under 0.12%, 0.24%, and 0.43% SS. Open circles and the solid line represent κ_{CCNC} plotted against κ_{HTDMA}^{*} and the regression line constrained through the origin, respectively.

analysis, similar ranges of $d_{p,dry}$ were selected for comparison because both values are size dependent (0.12% SS: 131–151 nm and 142 ± 11 nm, 0.24% SS: 88–102 nm and 95 ± 8 nm, and 0.43% SS: 64–74 nm and 69 ± 8 nm for κ_{HTDMA} and κ_{CCNC}, respectively). Whereas the ensemble of κ_{CCNC} under all SS conditions correlated strongly with the corresponding κ_{HTDMA} ($r = 0.90$, $p \ll 0.01$), the κ_{CCNC} was higher than κ_{HTDMA} and the degree of difference calculated from all data pairs at three SS ($n = 80$) was +37% ± 19%. The degree of difference is similar to that of urban aerosols in Germany (+37%) [*Wu et al.*, 2013]. One possible reason for the difference is the dependence of the κ value of chemical components on the concentration of the solution, i.e., the saturation ratio of water vapor. For example, according to the mean values for particles at d_{act} for three SSs, the κ value of ammonium sulfate particles under supersaturated conditions (0.60) is ~18% higher than that at 85% RH (0.51). To assess the effect of inorganic salts, the sum of κ_{HTDMA} and the estimated increase in κ under supersaturated conditions by the presence of inorganic salts was calculated as a hypothetical parameter κ_{HTDMA}^{*};

$$\kappa_{HTDMA}^{*} = \kappa_{HTDMA} + \varepsilon_{IS}(\kappa_{IS\_SS} - \kappa_{IS}) \quad (9)$$

Here κ_{IS} and κ_{IS_SS} are the κ values of the inorganic salt fraction at 85% RH and at 0.12%–0.43% SS, respectively, which are calculated from the κ values of ammonium sulfate and ammonium nitrate under the respective humidity conditions with the ZSR mixing rule. The κ_{IS} is the volume fraction of the salts (the sum of κ_{AS} and κ_{AN}). The mean values (ranges) of κ_{IS_SS} and κ_{IS} are 0.54 (0.52–0.56) at 85% RH and 0.63 (0.61–0.66) at 0.12%–0.43% SS, respectively; the κ values of inorganic salts under supersaturated conditions are ~20% higher than those at 85% RH. The values of κ_{HTDMA}^{*} and κ_{CCNC} are compared in Figure 10b and Table 3. A +28% ± 16% difference remains for κ_{HTDMA}^{*} and κ_{CCNC} based on the averages of the ratios of κ_{CCNC} to κ_{HTDMA}^{*} at three SS. Note that the large RH dependence of the κ value of inorganics may generally affect the comparison of κ under subsaturated conditions with that under supersaturated conditions. Both the Pitzer equation [*Pitzer and Mayorga*, 1973] and the equations in *Tang and Munkelwitz* [1994] indicate that the κ values of ammonium sulfate at ~90% RH are even lower than those at 85% RH.

It is likely that organics contribute to the remaining difference. Whereas some previous studies have reported that κ_{HTDMA} and κ_{CCNC} agree well (±20%, [*Carrico et al.*, 2008; *Duplissy et al.*, 2008]), discrepancies have been reported in other studies (20%–50% [*Massoli et al.*, 2010] and 37% [*Wu et al.*, 2013]). The reasons for the difference were discussed based on both laboratory and field studies; the reasons include a reduction of surface tension, the presence of sparingly soluble materials (<90% RH), and the insufficient expression of the dependence of the activity coefficient of water on the concentration of the solution at high RH (>95%)

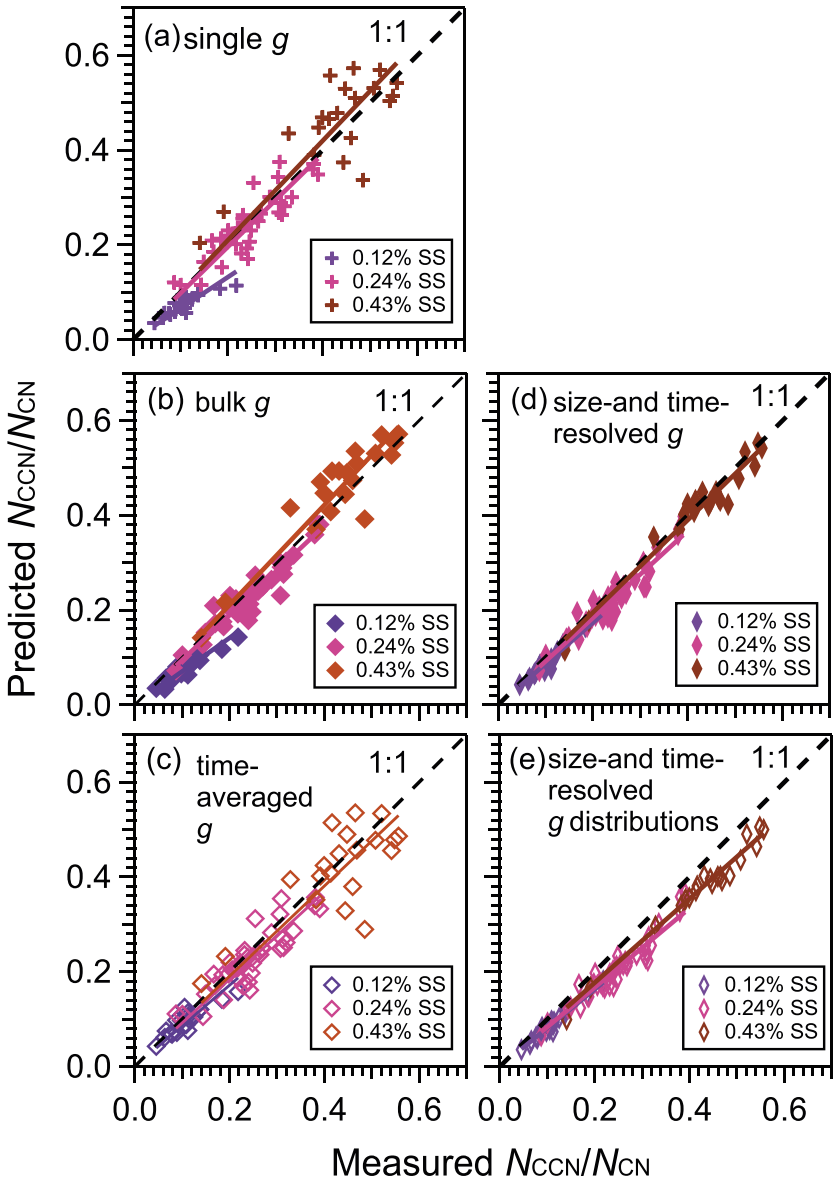

Figure 11. The N_{CCN}/N_{CN} values predicted with considerations of (a) single g, (b) size-averaged and time-resolved g, (c) time-averaged and size-resolved g, (d) size- and time-resolved g, and (e) size- and time-resolved g distributions versus the measured N_{CCN}/N_{CN}, for the size range of 24–359 nm. Solid lines represent the regression lines constrained through the origin.

[*Prenni et al.*, 2007; *Wex et al.*, 2009; *Good et al.*, 2010a, 2010b; *Massoli et al.*, 2010; *Kristensen et al.*, 2012]. The large fraction of organics obtained in this study might be preferable for inducing these effects of organics and may have resulted in the difference between $\kappa_{HTDMA}{}^{*}$ and κ_{CCNC}. Calculations with the assumption of internally mixed, spherical particles and the co-condensation of semivolatile compounds might have also caused the difference [*Dusek et al.*, 2011; *Jung et al.*, 2011; *Topping and McFiggans*, 2012]. Note that the ratio of $\kappa_{CCNC}/\kappa_{HTDMA}{}^{*}$ did not show strong correlation with κ_{HTDMA} ($r = -0.26$, $p = 0.03$). Hence, the relevance of the factors to the fraction of organics, which is related to κ_{HTDMA} (Figure 10), is not evident.

3.5. Importance of the Variations in Particle Hygroscopicity With Time and Size and the Hygroscopicity of Organics

N_{CCN}/N_{CN} values in the range of 24–359 nm were predicted and compared with the measured values to investigate the contributions of the variations in g with time and size and g distributions to N_{CCN}

Table 4. The Ratios of the Predicted N_{CCN}/N_{CN} to Measured N_{CCN}/N_{CN} Over the Range of 24–359 nm, With Different Considerations of g for Prediction[a]

SS	Single g	Time-Resolved g	Size-Resolved g	Size- and Time-Resolved g	Size- and Time-Resolved g Distributions
0.12%	0.70 (0.15)	0.73 (0.13)	0.91 (0.15)	0.86 (0.08)	0.81 (0.07)
0.24%	1.01 (0.15)	0.95 (0.10)	0.94 (0.15)	0.92 (0.10)	0.83 (0.09)
0.43%	1.10 (0.17)	1.07 (0.10)	0.99 (0.17)	0.97 (0.07)	0.88 (0.06)

[a]Values in parentheses are the relative standard deviations of the ratios of the predicted N_{CCN}/N_{CN} values to the measured values.

(Figures 11a–11e and Table 4). Although the predicted N_{CCN}/N_{CN} values roughly agree with the measured values if a size- and time-averaged g is used as a representative value (mean relative differences: −30% to +10% for three SS), the relative standard deviation (RSD) values are large (15% − 17%, Figure 11a and Table 4). When time-resolved but size-averaged g values are applied (Figure 11b), the mean relative differences in the predicted N_{CCN}/N_{CN} values from the measured values are not largely different (−27% to +7%), but the RSD values are smaller (10%–13%). If size-resolved but time-averaged g values are applied (Figure 11c), the RSD values are not largely different from those obtained using a size- and time-averaged g value (15%–17%), but the mean relative differences at 0.12% and 0.43% SS are much closer to zero (−9% to −1%). Additionally, smaller RSD values are obtained if time- and size-resolved g values are considered (7%–10%, Figure 11d) or if g distributions as well as their time and size dependence are fully considered (6%–9%, Figure 11e). Although the predicted N_{CCN}/N_{CN} are slightly underestimated in these cases, the large underestimation obtained when using single g and time-resolved g values at 0.12% SS improves. The above mentioned results indicate that the temporal variations and the size dependence of particle hygroscopicity largely controlled the CCN number concentrations. At 0.24% and 0.43% SS, the mean relative difference if g distributions are considered is substantially different from those if g distributions are not considered but time- and size-resolved g are considered, relative to the case at 0.12% SS. The result suggests that the mixing state is relatively more important at high SS [*Meng et al.*, 2014], although the consideration of g distributions enhances the underprediction in the present study.

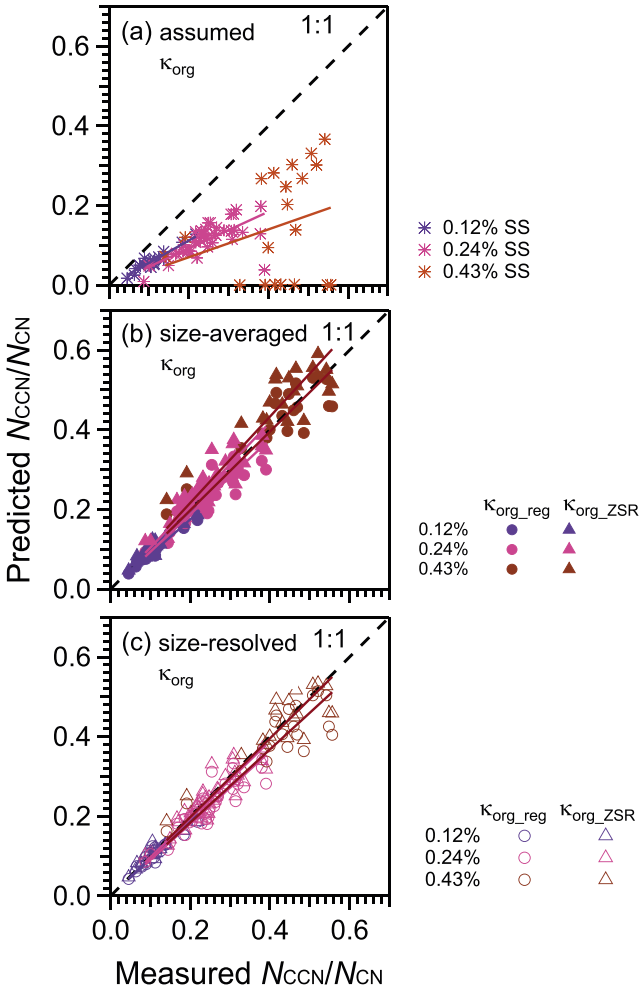

Figure 12. The N_{CCN}/N_{CN} values predicted with (a) a κ_{org} value of 0, (b) size-averaged κ_{org}, and (c) size-resolved κ_{org} versus the measured N_{CCN}/N_{CN} for the size range of 24–359 nm. Circles and triangles in Figures 12b and 12c represent values predicted from ε_{org}-derived κ_{org} by the regression analysis and ZSR-individual methods, respectively. Solid lines represent the regression lines constrained through the origin.

The contribution of the hygroscopicity of organics to N_{CCN}/N_{CN} in the range of 24–359 nm was also assessed, as

Table 5. The Ratios of the Predicted N_{CCN}/N_{CN} to Measured N_{CCN}/N_{CN} Over the Range of 24–359 nm, With Different Assumptions/Considerations of κ_{org} for Prediction[a]

		Bulk		Size Resolved	
SS	$\kappa_{org} = 0$	Regression	ZSR Individual	Regression	ZSR Individual
0.12%	0.55 (0.17)	0.90 (0.08)	0.98 (0.12)	0.97 (0.11)	1.02 (0.12)
0.24%	0.47 (0.25)	0.96 (0.11)	1.08 (0.13)	0.92 (0.12)	0.99 (0.12)
0.43%	0.36 (0.81)	1.03 (0.14)	1.14 (0.16)	0.95 (0.13)	1.03 (0.14)

[a]Values in parentheses are the relative standard deviations of the ratios of the predicted N_{CCN}/N_{CN} values to the measured values.

presented in Figures 12a–12c and Table 5. The predicted N_{CCN}/N_{CN} values are largely underestimated if κ_{org} is assumed to be zero, i.e., organics are insoluble (Figure 12a); the averages of the differences of the ratios of the predicted to the measured N_{CCN}/N_{CN} values from unity at 0.12%, 0.24%, and 0.43% SS (mean relative differences) range from −64% to −45% (Table 5). The RSD values of the ratios of the predicted to the measured N_{CCN}/N_{CN} for three SS range from 17% to 81%. If size-averaged κ_{org} values derived from the regression analysis (0.14) and the ZSR-individual method (0.19) are applied regardless of particle size, the mean relative differences for three SS become small (−10% to +3% and −2% to +14%, respectively, Figure 12b). Additionally, the RSD values also become small. When size-resolved κ_{org} values derived from the regression method (0.12–0.18) and the ZSR-individual method (0.14–0.23) are applied, the degree of consistency does not largely differ from those obtained using size-averaged κ_{org} values, but the mean relative differences are close to unity (Figure 12c). The greater consistency that occurs with consideration of κ_{org} estimated in this study suggests that organics were hygroscopic to some degree (section 3.3) and contributed to N_{CCN}. The results obtained with a κ_{org} value of zero indicate that the use of appropriate κ_{org} values is particularly important at a high SS, likely because the effect of the large organic fractions at small diameters overwhelms that of the relatively high sensitivity of N_{CCN} to particle hygroscopicity at a low SS [*Meng et al*., 2014]. Note that the predicted N_{CCN}/N_{CN} values agreed with the measured values with the mean relative differences from −18% to −9% and those from −2% to +17%, respectively, if κ_{org} values are assumed to be 0.1 and 0.2 based on a literature value of κ_{org} (0.1 ± 0.1) [*Rose et al*., 2010].

As discussed for the difference between $\kappa_{HTDMA}{}^{*}$ and κ_{CCNC}, the remaining ~15% differences in the cases involving time- and size-resolved g distributions (Figures 11e) may be explained by the effects associated with organics, i.e., their Kelvin effect (e.g., surface tension reduction) and Raoult effect (e.g., the dissolution of sparingly soluble materials with an increase in RH and the nonideal behavior of the solution), as well as other effects and measurement uncertainties. To assess these possibilities, the reduction of surface tension and the increase in κ with the change in water vapor conditions from subsaturation to supersaturation are assumed in the calculation of N_{CCN}/N_{CN}. The 15% difference in the CCN closure can be explained by the decrease in surface tension or a combination of the surface tension reduction and the enhanced solute effect. For example, ~11% surface tension reduction and a combination of <10% surface tension reduction and ~20% enhanced solute effect can explain the differences between the measured and predicted N_{CCN}/N_{CN} values. Note that the partitioning between the bulk and the surface of the surfactant is needed for the accurate estimation of the surface tension reduction [*Sorjamaa et al*., 2004; *Petters and Kreidenweis*, 2013; *Raatikainen and Laaksonen*, 2014]. However, this partitioning effect is not considered in this study because the assessment is difficult for ambient aerosols, in which the composition and amount of surfactants are unknown. The ~11% surface tension reduction is possible in the atmosphere, as reported in previous studies: The reduction in surface tension by organics in ambient aerosols has been reported to reach up to >20% [*Facchini et al*., 1999, 2000; *Fors et al*., 2010]. Additionally, an increase in the hygroscopicity of organics from subsaturated to supersaturated conditions may also be possible, as with inorganic salts, given that nonideal behavior of organic compounds has been reported [*Kreidenweis et al*., 2008].

The results obtained from the CCN closure suggest that the solubility of organics and the externally mixed condition of the aerosol must be considered for an accurate prediction of CCN number concentrations. This result is consistent with that obtained by *Ervens et al*. [2010]. The authors discussed the effect of chemical properties on the prediction of CCN at six different locations (both urban and remote sites) and suggested

that the size-resolved chemical composition or hygroscopicity of particles and organics, and the mixing state must be considered for predictions near particle sources (e.g., urban sites), whereas the prediction for remote sites is not affected by these considerations. Some studies also suggest that consideration of the presence of less hygroscopic particles (i.e., HOA or BC) and their degree of hygroscopicity and mixing state are important for the prediction of CCN at urban sites [*Cubison et al*., 2008; *Quinn et al*., 2008]. As in previous studies, the results of this study provide implications for modeling studies of CCN, particularly for urban aerosols.

4. Summary

The distributions of g, ratios of CCN to CN, chemical composition, and number-size distributions of aerosol particles were measured at an urban site in Nagoya, Japan. The average of the size-resolved g distributions at 85% RH was bimodal with less and more hygroscopic modes. The mean g_m and κ_{HTDMA} values for 24–359 nm particles were 1.27 and 0.22, respectively. The g_m and κ_{HTDMA} values were relatively low for small particles and larger at larger diameters. The Aitken mode range was dominated by particles that had relatively low hygroscopicity ($0.8 \leq g < 1.25$) and consisted of freshly emitted organic compounds. Conversely, the accumulation mode range was dominated by particles that had relatively high hygroscopicity ($1.25 \leq g \leq 2.2$) and consisted of oxidized organic compounds and inorganic salts. The size-averaged κ_{org} value at 60–359 nm and the mean from respective size ranges obtained by the regression method were calculated as 0.14 and 0.12–0.18, respectively. The mean κ_{org} from all four size ranges and the mean from respective size ranges obtained by the ZSR-individual method were calculated as 0.19 and 0.14–0.23, respectively. The κ_{org} values correlated positively with f_{44} and O/C, but their correlations were not high. The F_{act} values at 0.12%, 0.24%, and 0.43% SS were >0.9 in most cases during the observation period, indicating low fractions of CCN-inactive particles at large diameters. The mean κ_{CCNC} values calculated from d_{act} at 0.12%, 0.24%, and 0.43% SS were 0.32, 0.26, and 0.23, respectively, showing the size dependence that smaller particles had lower hygroscopicity, as observed for κ_{HTDMA}. The κ_{CCNC} value was 37% higher than the κ_{HTDMA} value, and 28% of 37% difference may have been due to the effects of organics, in addition to the simplifications made for the calculations of κ_{HTDMA} and κ_{CCNC}, and possible co-condensation of semivolatile organics.

In the CCN closure, the predicted N_{CCN}/N_{CN} values were consistent with the measured values with mean relative differences ranging from −30% to +10% (RSD: 15%–17%) if a representative single g value is considered. A greater consistency was obtained when size- and time-resolved g or size- and time-resolved g distributions are considered (mean relative differences: −19% to −3%, RSD: 6%–10%). This result indicates the importance of the dependence of g on time and size to N_{CCN}. The predicted N_{CCN}/N_{CN} values are largely underestimated (mean relative differences at three SS: −64% to −45%) if κ_{org} is assumed to be zero. Using size-averaged κ_{org} values (0.14 and 0.19) obtained from g, the predicted N_{CCN}/N_{CN} values were more consistent with the measured values with mean relative differences ranging from −10% to − +3% and those ranging from −2% to +14%, respectively. This result suggests that water-soluble organics substantially contributed to N_{CCN}. The remaining 15% difference of N_{CCN}/N_{CN} in the CCN closure with g distributions can be explained solely by a surface tension reduction (10%–12%) or by a combination of a surface tension reduction and an enhanced solute effect. The results obtained in this study demonstrate that the variations in particle hygroscopicity with time and size and the hygroscopicity of organics affect CCN number concentrations in an urban area.

Appendix A: Calculation of Hygroscopicity of Organics From κ_{CCNC}

The κ value of organics under supersaturated conditions, κ_{org_SS}, was calculated from κ_{CCNC}, similarly to the calculation of κ_{HTDMA}:

$$\kappa_{org\_SS} = \frac{\kappa_{CCNC} - \left(\kappa_{AS\_SS}\varepsilon_{AS} + \kappa_{AN\_SS}\varepsilon_{AN} + \kappa_{EC}\varepsilon_{EC}\right)}{\varepsilon_{org}}$$

The size-averaged κ_{org_SS} values were determined using the chemical composition of particles in the range of 69–256 nm in d_{va} for particles at d_{act} under 0.12%, 0.24%, and 0.43% SS conditions (69–142 nm). The size-resolved κ_{org_SS} values were determined using chemical compositions in the ranges of 75–119, 101–163, and 145–248 nm in d_{va} for particles at d_{act} of 69, 95, and 142 nm, respectively. The size-averaged and size-resolved κ_{org_SS} values obtained by the regression method were 0.19 and 0.17–0.23, respectively. The size-averaged and size-resolved mean κ_{org_SS} values obtained by the ZSR-individual method were 0.24 and

0.20–0.28, respectively. The calculated κ_{org_SS} values are weakly correlated ($r \sim 0.40$) with f_{44}, as observed for κ_{org} derived from κ_{HTDMA}. Using the CCNC-derived κ_{org_SS} in the CCN closure, a result similar to that obtained from HTDMA-derived κ_{org} in Figure 12 was obtained. The predicted N_{CCN}/N_{CN} in the range of 24–359 nm is largely underestimated if κ_{org_SS} is assumed to be zero (mean relative differences: −61% to −36%). If size-averaged (or size-resolved) κ_{org_SS} values obtained by the regression method are used, the predicted N_{CCN}/N_{CN} values are consistent with the measured values with mean relative differences ranging from 2% to +19% (or +2% to + 12%). If size-averaged (or size-resolved) κ_{org_SS} values obtained by the ZSR-individual method are used, the predicted N_{CCN}/N_{CN} values are consistent with the measured values with mean relative differences ranging from +1% to +27% (or +12% to +21%). This result suggests that organics contributed to the CCN activation, as observed based on the results from the HTDMA-derived κ_{org}.

Acknowledgments
We thank K. Osada for providing the SMPS. We also thank Murata Keisokuki Service Corp. for the analysis of ionic species, EC, and OC on filters. We acknowledge the National Oceanic and Atmospheric Administration (NOAA) Air Resources Laboratory (ARL) for the use of the HYbrid Single-Particle Lagrangian Integrated Trajectory (HYSPLIT) model. This study was supported in part by a Grant-in-Aid for Young Scientists (S) (20671001). The data used for this paper are available for free upon request from the corresponding author (mochida.michihiro@g.mbox.nagoya-u.ac.jp).

References

Ahlm, L., et al. (2012), Formation and growth of ultrafine particles from secondary sources in Bakersfield, California, *J. Geophys. Res.*, *117*, D00V08, doi:10.1029/2011JD017144.

Aiken, A. C., et al. (2008), O/C and OM/OC ratios of primary, secondary, and ambient organic aerosols with high-resolution time-of-flight aerosol mass spectrometry, *Environ. Sci. Technol.*, *42*, 4478–4485, doi:10.1021/es703009q.

Albrecht, B. A. (1989), Aerosols, cloud microphysics, and fractional cloudiness, *Science*, *245*, 1227–1230, doi:10.1126/science.245.4923.1227.

Alfarra, M. R., N. Good, K. P. Wyche, J. F. Hamilton, P. S. Monks, A. C. Lewis, and G. McFiggans (2013), Water uptake is independent of the inferred composition of secondary aerosols derived from multiple biogenic VOCs, *Atmos. Chem. Phys.*, *13*, 11,769–11,789, doi:10.5194/acp-13-11769-2013.

Andreae, M. O., and D. Rosenfeld (2008), Aerosol-cloud-precipitation interactions, Part 1. The nature and sources of cloud-active aerosols, *Earth Sci. Rev.*, 13–41.

Asa-Awuku, A., A. Nenes, S. Gao, R. C. Flagan, and J. H. Seinfeld (2010), Water-soluble SOA from allene ozonolysis: Composition and droplet activation kinetics inferences from analysis of CCN activity, *Atmos. Chem. Phys.*, *10*, 1585–1597, doi:10.5194/acp-10-1585-2010.

Bougiatioti, A., C. Fountoukis, N. Kalivitis, S. N. Pandis, A. Nenes, and N. Mihalopoulos (2009), Cloud condensation nuclei measurements in the marine boundary layer of the eastern Mediterranean: CCN closure and droplet growth kinetics, *Atmos. Chem. Phys.*, *9*, 7053–7066, doi:10.5194/acp-9-7053-2009.

Bougiatioti, A., A. Nenes, C. Fountoukis, N. Kalivitis, S. N. Pandis, and N. Mihalopoulos (2011), Size-resolved CCN distributions and activation kinetics of aged continental and marine aerosol, *Atmos. Chem. Phys.*, *11*, 8791–8808, doi:10.5194/acp-11-8791-2011.

Carrico, C. M., M. D. Petters, S. M. Kreidenweis, J. L. Collett Jr., G. Engling, and W. C. Malm (2008), Aerosol hygroscopicity and cloud droplet activation of extracts of filters from biomass burning experiments, *J. Geophys. Res.*, *113*, D08206, doi:10.1029/2007JD009274.

Chang, R. Y.-W., P. S. K. Liu, W. R. Leaitch, and J. P. D. Abbatt (2007), Comparison between measured and predicted CCN concentrations at Egbert, Ontario: Focus on the organic aerosol fraction at a semi-rural site, *Atmos. Environ.*, *41*, 8172–8182.

Chang, R. Y.-W., J. G. Slowik, N. C. Shantz, A. Vlasenko, J. Liggio, S. J. Sjostedt, W. R. Leaitch, and J. P. D. Abbatt (2010), The hygroscopicity parameter (κ) of ambient organic aerosol at a field site subject to biogenic and anthropogenic influences: Relationship to degree of aerosol oxidation, *Atmos. Chem. Phys.*, *10*, 5047–5064, doi:10.5194/acp-10-5047-2010.

Cubison, M. J., B. Ervens, G. Feingold, K. S. Docherty, I. M. Ulbrich, L. Shields, K. Prather, S. Hering, and J. L. Jimenez (2008), The influence of chemical composition and mixing state of Los Angeles urban aerosol on CCN number and cloud properties, *Atmos. Chem. Phys.*, *8*, 5649–5667, doi:10.5194/acp-8-5649-2008.

Decarlo, P. F., J. G. Slowik, D. R. Worsnop, P. Davidovits, and J. L. Jimenez (2004), Particle morphology and density characterization by combined mobility and aerodynamic diameter measurements, Part 1: Theory, *Aerosol Sci. Technol.*, *38*, 1185–1205, doi:10.1080/027868290903907.

Duplissy, J., et al. (2008), Cloud forming potential of secondary organic aerosol under near atmospheric conditions, *Geophys. Res. Lett.*, *35*, D03818, doi:10.1029/2007GL031075.

Duplissy, J., et al. (2011), Relating hygroscopicity and composition of organic aerosol particulate matter, *Atmos. Chem. Phys.*, *11*, 1155–1165, doi:10.5194/acp-11-1155-2011.

Dusek, U., G. P. Frank, A. Massling, K. Zeromskiene, Y. Iinuma, O. Schmid, G. Halas, T. Hennig, A. Wiedensohler, and M. O. Andreae (2011), Water uptake by biomass burning aerosol at sub- and supersaturated conditions: Closure studies and implications for the role of organics, *Atmos. Chem. Phys.*, *11*, 9519–9532, doi:10.5194/acp-11-9519-2011.

Ervens, B., M. Cubison, E. Andrews, G. Feingold, J. A. Ogren, J. L. Jimenez, P. DeCarlo, and A. Nenes (2007), Prediction of cloud condensation nucleus number concentration using measurements of aerosol size distributions and comparison and light scattering enhancement due to humidity, *J. Geophys. Res.*, *112*, D10S32, doi:10.1029/2006JD007426.

Ervens, B., et al. (2010), CCN predictions using simplified assumptions of organic aerosol composition and mixing state: A synthesis from six different locations, *Atmos. Chem. Phys.*, *10*, 4795–4807, doi:10.5194/acp-10-4795-2010.

Facchini, M. C., M. Mircea, S. Fuzzi, and R. J. Charlson (1999), Cloud albedo enhancement by surface-active organic solutes in growing droplets, *Nature*, *401*, 257–259, doi:10.1038/45758.

Facchini, M. C., S. Decesari, M. Mircea, S. Fuzzi, and G. Loglio (2000), Surface tension of atmospheric wet aerosol and cloud/fog droplets in relation to their organic carbon content and chemical composition, *Atmos. Environ.*, *34*, 4853–4857.

Fors, E. O., et al. (2010), Hygroscopic properties of Amazonian biomass burning and European background HULIS and investigation of their effects on surface tension with two models linking H-TDMA to CCNC data, *Atmos. Chem. Phys.*, *10*, 5625–5639, doi:10.5194/acp-10-5625-2010.

Fors, E. O., E. Swietlicki, B. Svenningsson, A. Kristensson, G. P. Frank, and M. Sporre (2011), Hygroscopic properties of the ambient aerosol in southern Sweden—A two year study, *Atmos. Chem. Phys.*, *11*, 8343–8361, doi:10.5194/acp-11-8343-2011.

Good, N., D. O. Topping, J. D. Allan, M. Flynn, E. Fuentes, M. Irwin, P. I. Williams, H. Coe, and G. McFiggans (2010a), Consistency between parameterizations of aerosol hygroscopicity and CCN activity during the RHaMBLe discovery cruise, *Atmos. Chem. Phys.*, *10*, 3189–3203, doi:10.5194/acp-10-3189-2010.

Good, N., et al. (2010b), Widening the gap between measurement and modelling of secondary organic aerosol properties?, *Atmos. Chem. Phys.*, *10*, 2577–2593, doi:10.5194/acp-10-2577-2010.
Gunthe, S. S., et al. (2011), Cloud condensation nuclei (CCN) from fresh and aged pollution in the megacity region of Beijing, *Atmos. Chem. Phys.*, *11*, 11,023–11,039, doi:10.5194/acp-11-11023-2011.
Hänel, G. (1976), The properties of atmospheric aerosol particles as functions of the relative humidity at thermodynamic equilibrium with the surrounding moist air, *Adv. Geophys.*, *17*, 73–188, doi:10.1016/S0065-2687(08)60142-9.
Jimenez, J. L., et al. (2009), Evolution of organic aerosols in the atmosphere, *Science*, *326*, 1525–1529, doi:10.1126/science.1180353.
Jung, J., Y. J. Kim, S. G. Aggarwal, and K. Kawamura (2011), Hygroscopic property of water-soluble organic-enriched aerosols in Ulaanbaatar, Mongolia during the cold winter of 2007, *Atmos. Environ.*, *45*, 2722–2729.
Jurányi, Z., M. Gysel, E. Weingartner, P. F. DeCarlo, L. Kammermann, and U. Baltensperger (2010), Measured and modeled cloud condensation nuclei number concentration at the high alpine site Jungfraujoch, *Atmos. Chem. Phys.*, *10*, 7891–7906, doi:10.5194/acp-10-7891-2010.
Jurányi, Z., T. Tritscher, M. Gysel, M. Laborde, L. Gomes, G. Roberts, U. Baltensperger, and E. Weingartner (2013), Hygroscopic mixing state of urban aerosol derived from size-resolved cloud condensation nuclei measurements during the MEGAPOLI campaign in Paris, *Atmos. Chem. Phys.*, *13*, 6431–6446, doi:10.5194/acp-13-6431-2013.
Kammermann, L., M. Gysel, E. Weingartner, H. Herich, D. J. Cziczo, T. Holst, B. Svenningsson, A. Arneth, and U. Baltensperger (2010), Subarctic atmospheric aerosol composition: 3. Measured and modeled properties of cloud condensation nuclei, *J. Geophys. Res.*, *115*, D04202, doi:10.1029/2009JD012447.
Kawana, K., N. Kuba, and M. Mochida (2014), Assessment of cloud condensation nucleus activation of urban aerosol particles with different hygroscopicity and the application to the cloud parcel model, *J. Geophys. Res. Atmos.*, *119*, 3352–3371, doi:10.1002/2013JD020827.
Kim, J. H., S. S. Yum, S. Shim, S.-C. Yoon, J. G. Hudson, J. Park, and S.-J. Lee (2011), On aerosol hygroscopicity, cloud condensation nuclei (CCN) spectra and critical supersaturation measured at two remote islands of Korea between 2006 and 2009, *Atmos. Chem. Phys.*, *11*, 12,627–12,645, doi:10.5194/acp-11-12627-2011.
Kreidenweis, S. M., M. D. Petters, and P. J. DeMott (2008), Single-parameter estimates of aerosol water content, *Environ. Res. Lett.*, *3*(3), 035002, doi:10.1088/1748-9326/3/3/035002.
Kristensen, T. B., et al. (2012), Hygroscopic growth and CCN activity of HULIS from different environments, *J. Geophys. Res.*, *117*, D22203, doi:10.1029/2012JD018249.
Kuwata, M., Y. Kondo, Y. Miyazaki, Y. Komazaki, H. H. Kim, S. S. Yum, H. Tanimoto, and H. Matsueda (2008), Cloud condensation nuclei activity at Jeju Island, Korea in spring 2005, *Atmos. Chem. Phys.*, *8*, 2933–2948, doi:10.5194/acp-8-2933-2008.
Lathem, T. L., A. J. Beyersdorf, K. L. Thornhill, E. L. Winstead, M. J. Cubison, A. Hecobian, J. L. Jimenez, R. J. Weber, B. E. Anderson, and A. Nenes (2013), Analysis of CCN activity of Arctic aerosol and Canadian biomass burning during summer 2008, *Atmos. Chem. Phys.*, *13*, 2735–2756, doi:10.5194/acp-13-2735-2013.
Liu, X., and J. Wang (2010), How important is organic aerosol hygroscopicity to aerosol indirect forcing?, *Environ. Res. Lett.*, *5*(4), 044010, doi:10.1088/1748-9326/5/4/044010.
Martin, M., R. Y.-W. Chang, B. Sierau, S. Sjogren, E. Swietlicki, J. P. D. Abbatt, C. Lesk, and U. Lohmann (2011), Cloud condensation nuclei closure study on summer arctic aerosol, *Atmos. Chem. Phys.*, *11*, 11,335–11,350, doi:10.5194/acp-11-11335-2011.
Massling, A., M. Stock, B. Wehner, Z. J. Wu, M. Hu, E. Brüggemann, T. Gnauk, H. Herrmann, and A. Wiedensohler (2009), Size segregated water uptake of the urban submicrometer aerosol in Beijing, *Atmos. Environ.*, *43*, 1578–1589.
Massoli, P., et al. (2010), Relationship between aerosol oxidation level and hygroscopic properties of laboratory generated secondary organic aerosol (SOA) particles, *Geophys. Res. Lett.*, *37*, L24801, doi:10.1029/2010GL045258.
McFiggans, G., et al. (2006), The effect of physical and chemical aerosol properties on warm cloud droplet activation, *Atmos. Chem. Phys.*, *6*, 2593–2649, doi:10.5194/acp-6-2593-2006.
Mei, F., A. Setyan, Q. Zhang, and J. Wang (2013a), CCN activity of organic aerosols observed downwind of urban emissions during CARES, *Atmos. Chem. Phys.*, *13*, 12,155–12,169, doi:10.5194/acp-13-12155-2013.
Mei, F., P. L. Hayes, A. Ortega, J. W. Taylor, J. D. Allan, J. Gilman, W. Kuster, J. de Gouw, J. L. Jimenez, and J. Wang (2013b), Droplet activation properties of organic aerosols observed at an urban site during CalNex-LA, *J. Geophys. Res. Atmos.*, *118*, 2903–2917, doi:10.1002/jgrd.50285.
Meng, J. W., M. C. Yeung, Y. J. Li, B. Y. L. Lee, and C. K. Chan (2014), Size-resolved cloud condensation nuclei (CCN) activity and closure analysis at the HKUST supersite in Hong Kong, *Atmos. Chem. Phys.*, *14*, 10,267–10,282, doi:10.5194/acp-14-10267-2014.
Mochida, M., T. Miyakawa, N. Takegawa, Y. Morino, K. Kawamura, and Y. Kondo (2008), Significant alteration in the hygroscopic properties of urban aerosol particles by the secondary formation of organics, *Geophys. Res. Lett.*, *35*, L02804, doi:10.1029/2007GL031310.
Mochida, M., C. Nishita-Hara, Y. Kitamori, S. G. Aggarwal, K. Kawamura, K. Miura, and A. Takami (2010), Size-segregated measurements of cloud condensation nucleus activity and hygroscopic growth for aerosols at Cape Hedo, Japan, in spring 2008, *J. Geophys. Res.*, *115*, D21207, doi:10.1029/2009JD013216.
Mochida, M., C. Nishita-Hara, H. Furutani, Y. Miyazaki, J. Jung, K. Kawamura, and M. Uematsu (2011), Hygroscopicity and cloud condensation nucleus activity of marine aerosol particles over the western North Pacific, *J. Geophys. Res.*, *116*, D06204, doi:10.1029/2010JD014759.
Moore, R. H., R. Bahreini, C. A. Brock, K. D. Froyd, J. Cozic, J. S. Holloway, A. M. Middlebrook, D. M. Murphy, and A. Nenes (2011), Hygroscopicity and composition of Alaskan Arctic CCN during April 2008, *Atmos. Chem. Phys.*, *11*, 11,807–11,825, doi:10.5194/acp-11-11807-2011.
Moore, R. H., K. Cerully, R. Bahreini, C. A. Brock, A. M. Middlebrook, and A. Nenes (2012), Hygroscopicity and composition of California CCN during summer 2010, *J. Geophys. Res.*, *117*, D00V12, doi:10.1029/2010JD017352.
Nakayama, T., Y. Ikeda, Y. Sawada, Y. Setoguchi, S. Ogawa, K. Kawana, M. Mochida, F. Ikemori, K. Matsumoto, and Y. Matsumi (2014), Properties of light-absorbing aerosols in the Nagoya urban area, Japan, in August 2011 and January 2012: Contributions of brown carbon and lensing effect, *J. Geophys. Res. Atmos.*, *119*, 12,721–12,739, doi:10.1002/2014JD021744.
Ng, N. L., et al. (2010), Organic aerosol components observed in Northern Hemispheric datasets from aerosol mass spectrometer, *Atmos. Chem. Phys.*, *10*, 4625–4641, doi:10.5194/acp-10-4625-2010.
Pang, Y., B. J. Turpin, and L. A. Gundel (2006), On the importance of organic oxygen for understanding organic aerosol particles, *Aerosol Sci. Technol.*, *40*, 128–133, doi:10.1080/02786820500423790.
Petters, M. D., and S. M. Kreidenweis (2007), A single parameter representation of hygroscopic growth and cloud condensation nucleus activity, *Atmos. Chem. Phys.*, *7*, 1961–1971, doi:10.5194/acp-7-1961-2007.
Petters, M. D., and S. M. Kreidenweis (2013), A single parameter representation of hygroscopic growth and cloud condensation nucleus activity—Part 3: Including surfactant partitioning, *Atmos. Chem. Phys.*, *13*, 1081–1091, doi:10.5194/acp-13-1081-2013.
Pitzer, K. S., and G. Mayorga (1973), Thermodynamics of electrolytes. 2. Activity and osmotic coefficients for strong electrolytes with one or both ions univalent, *J. Phys. Chem.*, *77*, 2300–2308.

Prenni, A. J., M. D. Petters, S. M. Kreidenweis, P. J. DeMott, and P. J. Ziemann (2007), Cloud droplet activation of secondary organic aerosol, *J. Geophys. Res.*, *112*, D10223, doi:10.1029/2006JD007963.
Pringle, K. J., H. Tost, A. Pozzer, U. Pöschl, and J. Lelieveld (2010), Global distribution of the effective aerosol hygroscopicity parameter for CCN activation, *Atmos. Chem. Phys.*, *10*, 5241–5255, doi:10.5194/acp-10-5241-2010.
Quinn, P. K., T. S. Bates, D. J. Coffman, and D. S. Covert (2008), Influence of particle size and chemistry on the cloud nucleating properties of aerosols, *Atmos. Chem. Phys.*, *8*, 1029–1042, doi:10.5194/acp-8-1029-2008.
Raatikainen, T., and A. Laaksonen (2014), Comment on "Changes in droplet surface tension the observed hygroscopicity of photochemically aged biomass burning aerosol", *Environ. Sci. Technol.*, *48*, 2082–2083, doi:10.1021/es404971u.
Rader, D. J., and P. H. McMurry (1986), Application of the tandem differential mobility analyzer to studies of droplet growth or evaporation, *J. Aerosol Sci.*, *17*(5), 771–787.
Ramanathan, V., P. J. Crutzen, J. T. Kiehl, and D. Rosenfeld (2001), Aerosol, climate, and the hydrological cycle, *Science*, *294*, 2119–2124.
Rickards, A. M. J., R. E. H. Miles, J. F. Davies, F. H. Marshall, and J. P. Reid (2013), Measurement of the sensitivity of aerosol hygroscopicity and the κ parameter to the O/C ratio, *J. Phys. Chem. A*, *117*(51), 14,120–14,131, doi:10.1021/jp407991n.
Rissler, J., E. Swietlicki, J. Zhou, G. Roberts, M. O. Andreae, L. V. Gatti, and P. Artaxo (2004), Physical properties of the sub-micrometer aerosol over the Amazon rain forest during the wet-to-dry season transition-comparison of modeled and measured CCN concentrations, *Atmos. Chem. Phys.*, *4*, 2119–2143, doi:10.5194/acp-4-2119-2004.
Rose, D., S. S. Gunthe, E. Mikhailov, G. P. Frank, U. Dusek, M. O. Andreae, and U. Pöschl (2008), Calibration and measurement uncertainties of a continuous-flow cloud condensation nuclei counter(DMT-CCNC): CCN activation of ammonium sulfate and sodium chloride aerosol particles in theory and experiment, *Atmos. Chem. Phys.*, *8*, 1153–1179, doi:10.5194/acp-8-1153-2008.
Rose, D., A. Nowak, P. Achtert, A. Wiedensohler, M. Hu, M. Shao, Y. Zhang, M. O. Andreae, and U. Pöschl (2010), Cloud condensation nuclei in polluted air and biomass burning smoke near the mega-city Guangzhou, China—Part 1: Size-resolved measurements and implications for the modeling of aerosol particle hygroscopicity and CCN activity, *Atmos. Chem. Phys.*, *10*, 3365–3383, doi:10.5194/acp-10-3365-2010.
Rose, D., et al. (2011), Cloud condensation nuclei in polluted air and biomass burning smoke near the mega-city Guangzhou, China—Part 2: Size-resolved aerosol chemical composition, diurnal cycles, and externally mixed weakly CCN-active soot particles, *Atmos. Chem. Phys.*, *11*, 2817–2836, doi:10.5194/acp-11-2817-2011.
Salma, I., T. Borsós, T. Weidinger, P. Aalto, T. Hussein, M. Dal Maso, and M. Kulmala (2011), Production, growth and properties of ultrafine atmospheric aerosol particles in an urban environment, *Atmos. Chem. Phys.*, *11*, 1339–1353, doi:10.5194/acp-11-1339-2011.
Shinozuka, Y., et al. (2009), Aerosol optical properties relevant to regional remote sensing of CCN activity and links to their organic mass fraction: Airborne observations over central Mexico and the US west coast during MILAGRO/INTEX-B, *Atmos. Chem. Phys.*, *9*, 6727–6742, doi:10.5194/acp-9-6727-2009.
Sorjamaa, R., B. Svenningsson, T. Raatikainen, S. Henning, M. Bilde, and A. Laaksonen (2004), The role of surfactants in Köhler theory reconsidered, *Atmos. Chem. Phys.*, *4*, 2107–2117, doi:10.5194/acp-4-2107-2004.
Stolzenburg, N. R. (1988), An ultrafine aerosol size distribution measuring system, PhD thesis, Univ. of Minnesota, Minneapolis.
Takegawa, N., T. Miyakawa, Y. Kondo, J. L. Jimenez, Q. Zhang, D. R. Worsnop, and M. Fukuda (2006), Seasonal and diurnal variations of submicron organic aerosol in Tokyo observed using the Aerodyne aerosol mass spectrometer, *J. Geophys. Res.*, *111*, D11206, doi:10.1029/2005JD006515.
Tang, I. N., and H. R. Munkelwitz (1994), Water activities, densities, and refractive indices of aqueous sulfates and sodium nitrate droplets of atmospheric importance, *J. Geophys. Res.*, *99*, 18,801–18,808, doi:10.1029/94JD01345.
Topping, D. O., and G. McFiggans (2012), Tight coupling of particle size, number and composition in atmospheric cloud droplet activation, *Atmos. Chem. Phys.*, *12*, 3253–3260, doi:10.5194/acp-12-3253-2012.
Turpin, B. J., and H.-J. Lim (2001), Species contributions to PM2.5 mass concentrations: Revisiting common assumptions for estimating organic mass, *Aerosol Sci. Technol.*, *35*, 602–610.
Twomey, S. A. (1977), The influence of pollution on the shortwave albedo of clouds, *J. Atmos. Sci.*, *34*, 1149–1152.
Wang, J., Y.-N. Lee, P. H. Daum, J. Jayne, and M. L. Alexander (2008), Effects of aerosol organics on cloud condensation nucleus (CCN) concentration and first indirect aerosol effect, *Atmos. Chem. Phys.*, *8*, 6325–6339, doi:10.5194/acp-8-6325-2008.
Wex, H., M. D. Petters, C. M. Carrico, E. Hallbauer, A. Massling, G. R. McMeeking, L. Poulain, Z. Wu, S. M. Kreidenweis, and F. Stratmann (2009), Towards closing the gap between hygroscopic growth and activation for secondary organic aerosol: Part 1—Evidence from measurements, *Atmos. Chem. Phys.*, *9*, 3987–3997, doi:10.5194/acp-9-3987-2009.
Wex, H., G. McFiggans, S. Henning, and F. Stratmann (2010), Influence of the external mixing state of atmospheric aerosol on derived CCN number concentrations, *Geophys. Res. Lett.*, *37*, L10805, doi:10.1029/2010GL043337.
Wu, Z. J., et al. (2013), Relating particle hygroscopicity and CCN activity to chemical composition during the HCCT-2010 field campaign, *Atmos. Chem. Phys.*, *13*, 7983–7996, doi:10.5194/acp-13-7983-2013.
Yeung, M. C., B. P. Lee, Y. J. Li, and C. K. Chan (2014), Simultaneous HTDMA and HR-ToF-AMS measurements at the HKUST supersite in Hong Kong in 2011, *J. Geophys. Res. Atmos.*, *119*, 9864–9883, doi:10.1002/2013JD021146.
Zhang, Q., M. R. Canagaratna, J. T. Jayne, D. R. Worsnop, and J.-L. Jimenez (2005a), Deconvolution and quantification of hydrocarbon-like and oxygenated organic aerosols based on aerosol mass spectrometry, *Environ. Sci. Technol.*, *39*, 4938–4952.
Zhang, Q., D. R. Worsnop, M. R. Canagaratna, and J.-L. Jimenez (2005b), Hydrocarbon-like and oxygenated aerosols in Pittsburgh: Insights into sources and processes of organic aerosols, *Atmos. Chem. Phys.*, *5*, 3289–3311.
Zhang, Q., et al. (2007), Ubiquity and dominance of oxygenated species in organic aerosols in anthropogenically-influenced Northern Hemisphere midlatitudes, *Geophys. Res. Lett.*, *34*, L13801, doi:10.1029/2007GL029979.

Erratum

In the originally published version of this article, all of "F_{max}" in section 2.2 (including equation (3)) and Figure 9 (including the caption) should have been "F_{act}". This has since been corrected, and this version may be considered the authoritative version of record.